MS/SIM 20101053 Hyeong-Won Jeon (전형원). Network Coding for Multiple Sensor Networks on Underwater Acoustic Channels (수중음향채널에서의 다중센서네트워크를 위한 네트워크코딩).

School of Information and Mechatronics. 2012. 53p. Prof. Heung-No Lee

Abstract

The underwater acoustic channel (UAC) is known to offer poor communications channel. The channel medium is highly absorptive and the transmission bandwidth is limited. In addition, the channel is highly frequency selective; the degree of selectiveness depends on a detailed geometry of the channel. Further, the response changes over time as conditions affecting the response (such as water temperature, sea surface wind, salinity, etc.) are time-varying.

A system design to deal with the frequency and time selective channel in UAC, therefore, becomes very challenging. It has been known that deep fading at certain specific sub-carriers are detrimental to orthogonal frequency division multiplexing (OFDM) systems. To mitigate this negative effect, we considered low density parity check (LDPC) coded OFDM system to deal with deep sub-band fading problems. Further, to apply to multiple sensor networks and realistic channel, we used spatial domain coding technique, i.e., low density generator matrix (LDGM) code, and combine with LDPC coded OFDM system. Finally we showed the robust performance of our designed LDPC-LDGM coded OFDM system under realistic channel settings.

Contents

List of Tables

List of Figures

1 Introduction to Communication System Design over Underwater Acoustic Channel

1.1 Underwater Communications

The water composing most of earth is called as the origin of life. Human beings have had a close relationship with such water and tried to use efficiently. Recently, as interest increases in marine resources and environment, underwater communication is obtaining popularity for a variety of applications and expanding this research area beyond just the previous military surveillance. In specially, the monitoring for global warming and radiation leak were a hot issue, lately. There are a number of the expected effects by achieving the feasible underwater communication as follows [1].

- Monitoring of ocean environments – Underwater sensor networks can help correcting ocean environment data (i.e., ocean currents, winds, salinity, temperature, etc). It can help improving weather forecast and detecting climate change; understanding and predicting the effect of human ocean activity, as well as leisure activities, on marine ecosystems; monitoring distribution and tracking of fishes and microorganism, as well as marine pollution.

- Ocean survey – Underwater sensor networks can help scanning and analyzing ocean bottom geometry. It can be used to determine routes to install underwater cables and pipes; detecting underwater oilfields and reservoirs; exploring valuable minerals.

- Assisted navigation – Underwater sensor networks can be used to identify location of dangerous rocks in shallow waters, seaweed positions, submerged wrecked ship. It can serve benefits on safety, as well as academic data.

- Disaster prevention – Underwater sensor networks that is installed nearby trench or submarine volcano can provide warnings of submarine earthquakes and tsunami to coastal area. Further, it can observe leak of radiation or oil.

- Military surveillance – Underwater sensor networks can collaboratively monitor for surveillance, reconnaissance. In specially, it is useful for observing movement of submarine, torpedoes and mine.

1.2 Design Problem over Underwater Channel

In such potentiality and benefits, researchers have studied underwater communication techniques and tried to implement system, which attempts from 1970s to nowadays was well described in [2][3].

As shown Figure 1.1, the number of paper related underwater communications have been increase steadily, but there is limited number of papers against wireless sensor network over radio frequency (RF) channels since variety characteristics of underwater channel. One of the most effective reasons is basic carrier conveying information [4]. Among the carriers such as acoustic, electromagnetic (EM) and optical waves, most feasible carrier to transmit information in underwater is acoustic wave. By comparing with the features of acoustic wave and other carriers, why the acoustic wave primarily has been used is drawn as follows.

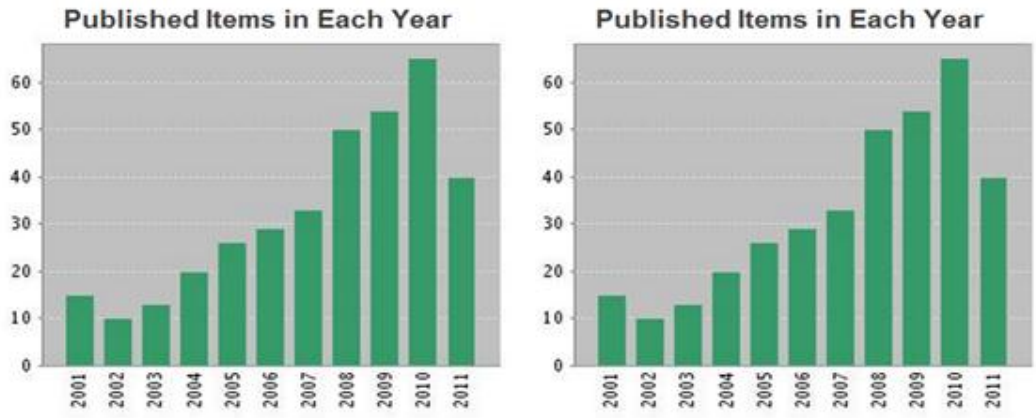

Figure 1.1 Number of published papers and citations
(Keyword : underwater acoustic communications)

- Acoustic Waves - So far, acoustic waves have been staying as the major carrier of wireless underwater communication. Acoustic communication is the most feasible and widely used in underwater environments due to the low attenuation. On the other hand, the use of acoustic waves in shallow water can be adversely affected by ambient noise and multipath propagation due to reflection and refraction. The much slower speed of acoustic propagation, i.e., 1,500 m/s, compared with that of EM and optical waves, is another limiting factor for efficient communication and networking, i.e., long guard time in system.

- Electromagnetic Waves - For EM wave carriers in water, the main shortcoming is the high absorption, especially in seawater. EM waves that are conventionally used in RF channel cannot work well in underwater environment owing to conducting nature of the medium. Nevertheless, EM waves works in underwater over only short distances, i.e., within 100 m. It is too short range to implement multiple sensor networks, thus it will still be a long way to expand the approach to be used in underwater sensor networks.

- Optical Waves - Optical wave carriers are generally limited to very short distances due to the serious water absorption at the optical frequency band. The clearest water has 1,000 times the attenuation of clean air and turbid water has more than 100 times the attenuation of the densest fog. In such reason, underwater optical communications only offers over very short range (10-100 m) with wide bandwidth (10-150 MHz). Optical carriers will remain as to be used for some special applications. The major hurdle is that optical communication in water is largely constrained by environments.

Table 1.1 shows the major characteristics summarization of acoustic, EM and optical waves [5]. Because of reason in terms of attenuation and transmission range, acoustic wave is the most suitable carrier for underwater environment.

As using acoustic wave as a carrier, the system should be considered that the multipath delay spread that comes from the reflection causes inter-symbol interference (ISI) and frequency selective fading, consequently leading to system performance falloff. Furthermore, the time selective fading and the Doppler spread caused by time-varying sea surface wind and moving fluids instigate system performance degradation [6][7]. Besides, channel conditions affecting the response (e.g., water temperature, sea surface wind and salinity) are time-varying.

There have been papers using the binary LDPC codes [8] and non-binary LDPC codes [9] in OFDM systems over such UAC. However, in these previous works, there were many cases using channel models that were overly simplified to test the system performance, e.g., (*i*) employing too little multipath components; (*ii*) overlooking the channel variation according to the positional change in the configuration of the node and buoy.

In this paper, we aim to (*i*) model a realistic simulation channel based on characteristics analysis of UAC; (*ii*) design an LDPC coded OFDM system to peer-to-peer communications. This system design can overcome the frequency selective fading, as well as time selective fading problems at the same time (within a 15 m/s maximum sea surface wind speed); and (*iii*) expand to sensor networks via user cooperation LDGM codes. Finally we show the robust performance of our designed LDPC-LDGM coded OFDM system under realistic channel settings.

Table 1.1 Comparison of acoustic, EM and optical waves in underwater

	Acoustic	**EM**	**Optical**
Speed (m/s)	~ 1,500	~ 33,333,333	~ 33,333,333
Attenuation	> 0.1 dB/m/Hz	~ 28 dB/km/100MHz	α turbidity
Bandwidth	~ kHz	~ MHz	~ 10-150 MHz
Frequency band	~ kHz	~ MHz	~ 10^{14}-10^{15} Hz
Major hurdles	Bandwidth limited Interference limited	Power limited	Environment limited
Data Rate	up to 100 kbps	up to 10 Mbps	up to 1Gbps
Transmission range	~ 50m-5km	~ 1m-100m	~ 1m-100m

1.3 Thesis Outline

The rest of the paper is organized as follows. In Section Ⅱ, we describe the channel modeling based on characteristics analysis of underwater acoustic channel. In Section Ⅲ, we introduce OFDM system in UAC, set the OFDM parameters to overcome ISI, frequency selective fading and time selective fading. Further, we show combining LDPC codes with OFDM system to mitigate negative deep fading effects. To apply to realistic system, we expand designed system to multiple sensor networks with LDGM codes in Section Ⅳ. We provide computer simulation results in Section Ⅴ, and summarize.

2 Channel Analysis and Modeling

2.1 Path Loss

The Path loss is one of the most distinguished characteristic of UAC. In the UAC, the path loss is affected by not only distance between transmitter and receiver but also carrier frequency [10]. The path loss of a signal with frequency f [Hz] over distance l [m] is

$$A(l, f) = A_0 \cdot l^k \cdot a(f)^l. \tag{2.1}$$

In (2.1), A_0 is a constant scaling factor and k is a spreading factor between 1 and 2, according to the type of spreading (In the case of cylindrical spreading, $k = 1$; practical spreading case, $k = 1.5$; spherical spreading case, $k = 2$). In this paper, we set A_0 as 1 and k as 2, considering spherical spreading. The absorption coefficient $a(f)$ denoting attenuation per each meter is

$$a(f) = 10^{\alpha(f/1000)/10000}, \tag{2.2}$$

where $\alpha(f)$ is approximated by Thorp's empirical formula [11].

$$a(f)[\text{dB/km}] = \begin{cases} 0.11\dfrac{f^2}{1+f^2} + 44\dfrac{f^2}{4100+f^2} + 2.75\cdot 10^{-4} f^2 + 0.003, & f \geq 0.4 \\ 0.002 + 0.11\dfrac{f^2}{1+f^2} + 0.011 f^2, & f < 0.4 \end{cases} \tag{2.3}$$

As compared with free-space path loss in RF channels like as (2.4) [12], although the path loss in RF channels is also affected by not only distance but also carrier frequency, the path loss in UAC is affect by carrier frequency more hugely.

$$A(l, f)[\text{dB}] = 32.4 + 20\log f[\text{MHz}] + 20\log l[\text{km}] \tag{2.4}$$

2.2 Ambient Noise

Similar to path loss, noise level depends on carrier frequency, as well as distance. In addition, noise is classified as site-specific noise and ambient noise. Site-specific noise exists only in certain place, whereas ambient noise exists all in deep-water area. Such ambient noise is composed of four major factors, which are turbulence noise, shipping noise, wave noise (wind noise) and thermal noise, each with different influential frequency range [13]. Each power spectral density (PSD) of factors is as follows.

Turbulence noise (< 10 Hz) : $10\log N_t(f) = 17 - 30\log f$

Shipping noise (10 ~ 100 Hz) : $10\log N_s(f) = 40 + 20(s - 0.5) + 26\log f - 60\log(f + 0.03)$

Wave noise (100 Hz ~ 100 kHz) : $10\log N_w(f) = 50 + 7.5w^{1/2} + 20\log f - 40\log(f + 0.4)$

Thermal noise (>100 kHz) : $10\log N_{th}(f) = -15 + 20\log f$,

where f is carrier frequency having kHz unit; s is shipping activity factor from 0 to 1; w is maximum wind speed on the sea surface having m/s unit.

Turbulence noise N_t caused by turbulent flow affects on only narrowband (f < 10 Hz) and shipping noise N_s caused by many unspecified ship affects the range from 10 to 100 Hz. Contrastively, wave noise N_w caused by sea surface wind and thermal noise N_{th} affect on broadband (100 Hz ~ 100 kHz) and over 100 kHz, respectively.

The PSD of ambient noise can be represented as a superposition of all factors as (2.5). Figure 2.1 shows such combined PDS of ambient noise according to wind speed and shipping activity factor.

$$N(f) = N_t(f) + N_s(f) + N_w(f) + N_{th}(f) \tag{2.5}$$

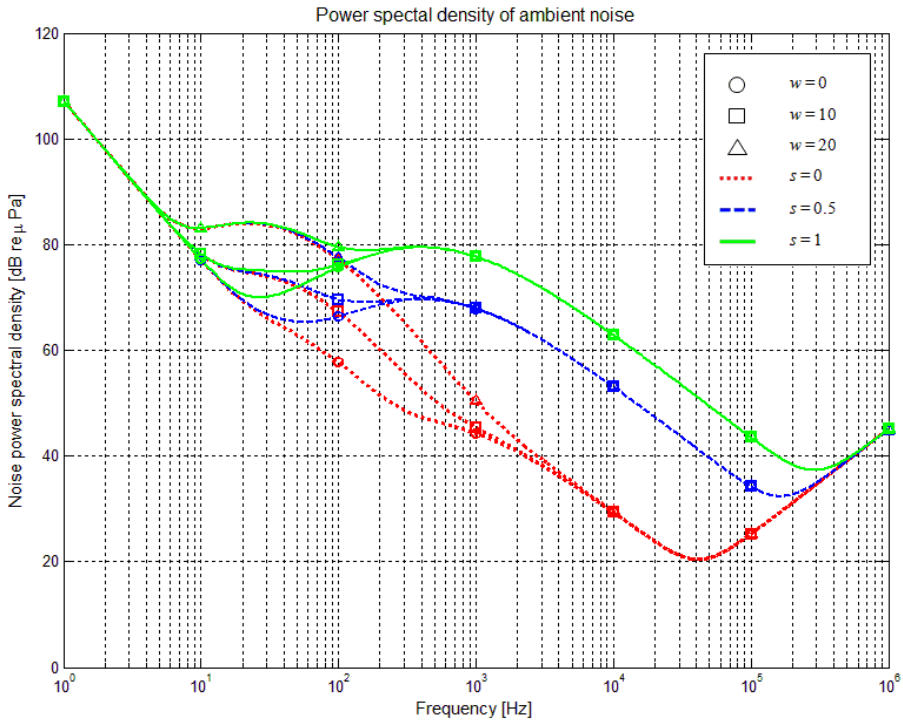

Figure 2.1 PSD of ambient noise

2.3 Doppler Spread

The surface scattering of UAC depends on the sea surface condition. Under an ideally flat surface condition, incident waves are almost perfectly reflected with π phase shifting, but, under practical conditions, swells lead to movement of the reflection point and create energy dispersion. The Doppler spread with a carrier frequency f [Hz] is represented as follows [14].

$$f_D = (0.0175/c) f \cdot w^{3/2} \cdot \cos\theta, \tag{2.6}$$

where c, w and θ are sound speed, sea surface wind speed and grazing angle, respectively. Sound speed in the water is affected by salinity, temperature, pressure, etc., but it is 1,500 m/s as the typical value under normal conditions.

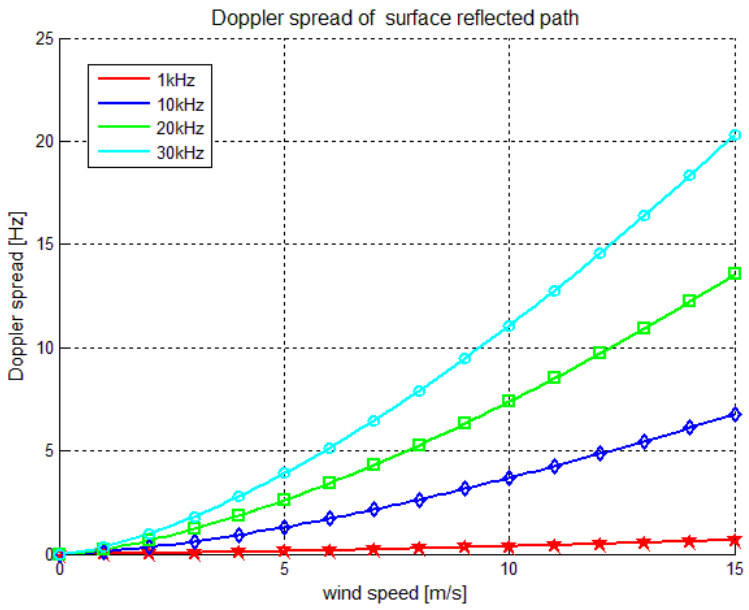

Figure 2.2 Doppler spread

Figure 2.2 is maximum Doppler spread according to carrier frequency and sea surface wind speed when we assumed $\cos\theta = 1$ in (2.6). This figure denotes a geometric Doppler spread increase as using a higher carrier frequency.

2.4 Trade-off between available Bandwidth and Doppler Spread

The signal-to-noise ratio (SNR) at the receiver is calculable as (2.7) by blending the path loss and ambient noise mentioned above section 2.1 and 2.2 [15].

$$SNR(l, f) = \frac{P / A(l, f)}{N(f)\Delta f}, \tag{2.7}$$

where P is transmit power.

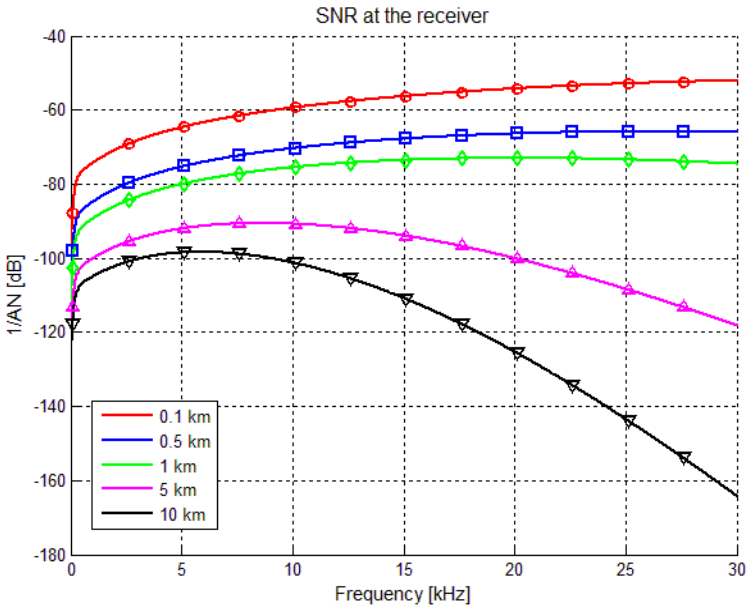

Figure 2.3 SNR at the receiver

Figure 2.3 shows the available bandwidth according to carrier frequency as a SNR at the receiver. For example, under assuming distance between transmitter and receiver is 1 km and energy cut is -80 dB, we are able to obtain 10 kHz bandwidth (from 5 kHz to 15 kHz) in case of 10 kHz carrier frequency. However, 30 kHz bandwidth (from 5 kHz to 35 kHz) is available if we set the carrier frequency as 20 kHz. This result means that as increase carrier frequency, we can use the wider bandwidth. However, there is a disadvantage either, i.e., geometric Doppler spread increase like as shown in Figure 2.2.

Although using a higher carrier frequency has an advantage (i.e., increases the available transmission bandwidth), it also has a disadvantage (i.e., increases geometric Doppler spread). Consequently, such trade-off relationship between available transmission bandwidth and Doppler spread according to carrier frequency should be considered on the communication system design over UAC.

2.5 Multipath

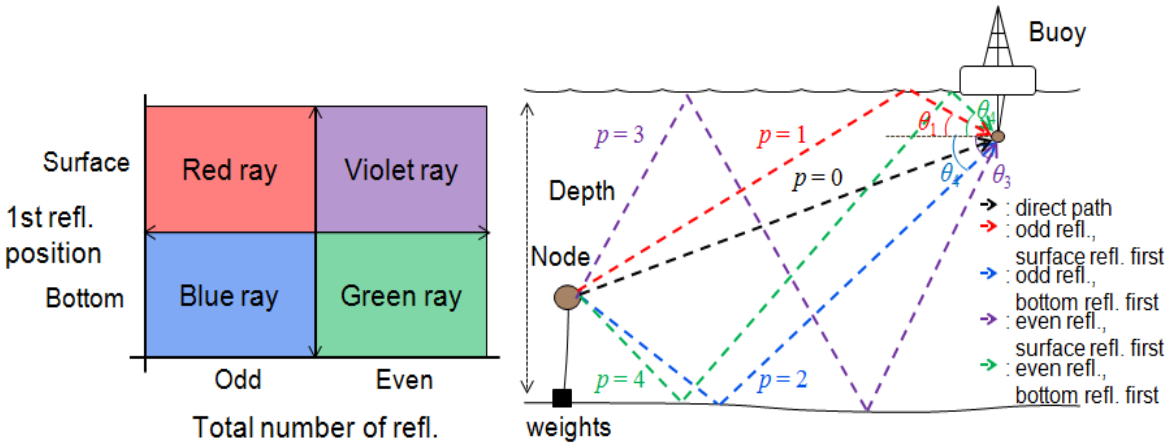

Figure 2.4 Multipath in UAC

UAC is extremely complex and difficult, since the conditions affecting the channel (such as geometry of the channel, wave height changed by sea surface wind, spatial position changed by sea current, etc.) need to be considered [16]. However, there are many problems and difficulties in applying all conditions to channel modeling. In this paper, the channel is modeled assuming almost flat surface and bottom conditions.

As shown in Figure 2.4, the acoustic waves in UAC are reflected on the sea surface and ocean bottom, as well as forming multipath [7]. Each reflection path is classified into four types based on two bases, i.e., total number of reflection times (odd number or even number) and the position occurred first reflection (sea surface or ocean bottom).

Figure 2.5 shows such classification according to total number of reflection. Figure 2.5 (a) shows the multipath having an odd number of reflections. The red ray (i) is a case where the first reflection occurred on the sea surface and blue ray (ii) is a case where the first reflection occurred on the ocean bottom. Similarly, Figure 2.5 (b) shows the multipath having an even number of reflections. In violet ray (iii) and green ray (iv), the first reflection occurred on the sea surface and ocean bottom.

These rays can be limited in the special cases. In the case of buoy is located on the ocean bottom, blue ray (ii) and green ray (iv) are limited. Similarly, red ray (i) and green ray (iv) cannot be created when buoy is located on the sea surface. Finally, in the case of node and buoy are located on the ocean bottom and sea surface, individually, there is only one creatable ray, i.e., violet ray (iii). Such limitation causes change of impulse response and wide performance variation.

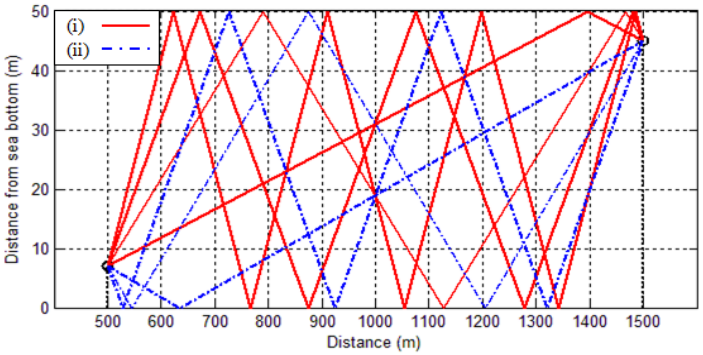

(a) Multipath having odd number reflection

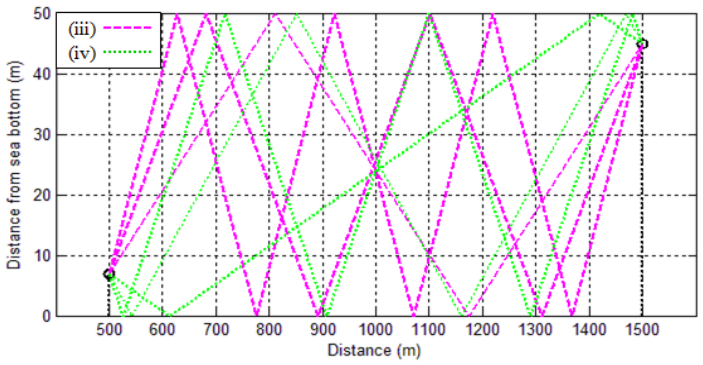

(b) Multipath having even number reflection

Figure 2.5 Multipath creation in UAC

2.6 Frequency response and Impulse response

The frequency response of each path is represented as function of frequency, number of reflection and distance of the path. The frequency response of the *p*-th path is

$$\bar{H}_p(f) = \frac{\Gamma_p}{\sqrt{A(l_p, f)}}, \tag{2.8}$$

where $A(l_p, f)$ is the single path loss with distance l_p [m] and carrier frequency f [Hz]. In addition, Γ_p is reflection coefficient, which is calculated using the number of times a path reflected from sea surface (n_{sp}) and from ocean bottom (n_{bp}) [17].

In (2.8), the reflection coefficient Γ_p is

$$\Gamma_p = \gamma_s^{n_{sp}} \gamma_b^{n_{bp}}(\theta_p), \tag{2.9}$$

where γ_s and γ_b are the reflection coefficients at the sea surface and ocean bottom, respectively. Under an ideally flat surface condition, γ_s is approximated as -1 and γ_b is calculated as follows.

$$\gamma_b(\theta) = \begin{cases} \dfrac{\rho_b \sin\theta - \rho\sqrt{(c/c_b)^2 - \cos^2\theta}}{\rho_b \sin\theta + \rho\sqrt{(c/c_b)^2 - \cos^2\theta}} & , \cos\theta \le c/c_b \\ 1 & otherwise \end{cases}, \tag{2.10}$$

where ρ and c are typical water density and sound speed values, i.e., 1,000 g/m^3 and 1,500 m/s. Similarly, ρ_b and c_b are typical values at the sea bottom, i.e., 1,800 g/m^3 and 1,300 m/s, respectively.

The impulse response of UAC with considering such reflection characteristic can be modeled as

$$h(t) = \sum_p h_p(t - \tau_p), \tag{2.11}$$

where h_p is an inverse Fourier Transform of *p*-th path frequency response and $\tau_p = (l_p - l_0)/c$ is an arrival time difference between direct path and the each *p*-th path.

3 Peer-to-Peer Communication Design

3.1 Simulation Channel Model

3.1.1 Simulation Channel Setting

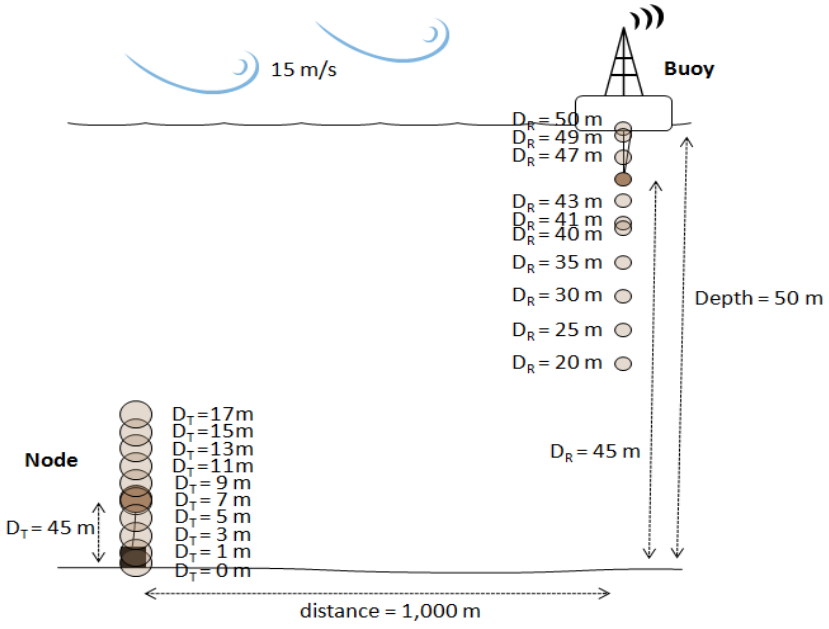

Figure 3.1 Simulation channel model

As we mentioned before, UAC modeling is extremely complex and difficult, since the conditions affecting the channel need to be considered. Thus, there are many problems and difficulties in applying all conditions to channel modeling. Actually, there is only limited number of paper that tried to consider such all conditions to channel modeling like as [16]. However, since it is too complex, they made many assumptions to reduce the complexity and make easy to analysis.

In this paper, the simulation channel is modeled under assuming almost flat surface and bottom conditions. In addition, simulation channel model has a water depth of 50 m and a maximum sea surface wind speed of 15 m/s, with 1,000 m separating the node and buoy as shown in Figure 3.1.

We selected following parameter to be aimed for designing over realistic condition. In specially, 50 m depth is approximated with considering average depth of the western sea, i.e., 44 m. As an original case, we set the node and buoy at 7 m and 45 m from ocean bottom, respectively. In addition, we assumed the node and buoy can be located at the various depths to observe performance variation according to channel changes. As details, node can be located at one of [0, 1, 3, 5, 9, 11, 13, 15, 17] m, as well as 7 m. In the case of buoy, possible located depth is one of [20, 25, 30, 34, 40, 41, 43, 47, 49, 50] m, as well as 45 m.

3.1.2 Simulation Channel Modeling

As shown in Figure 2.4, multipath is classified into four types based on two bases, i.e., total number of reflection times (odd number or even number) and the position occurred first reflection (surface or bottom).

It is necessary to calculate the distance of each reflection path since frequency response aforementioned section 2.6 is composed of function of carrier frequency, total number of reflections and distance of the path. To calculate the distance, we used the Pythagorean Theorem as follows.

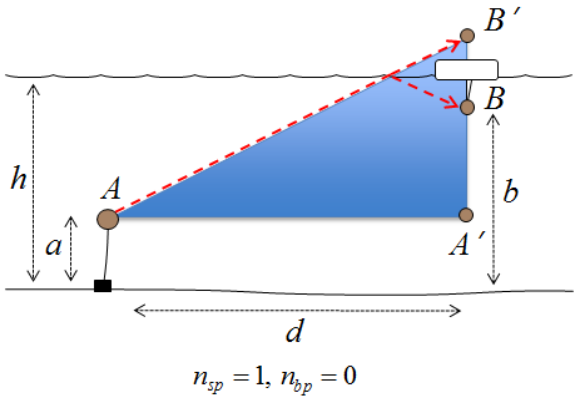

Figure 3.2 Example of reflection path

To calculate the distance,

1) Move B point to B' point against the sea surface.

2) Calculate the base line of triangle, i.e., d.

3) Calculate the height of triangle, i.e., $2h-a-b$.

   Since the distance from surface to A' is $h-a$ and from surface to B' is $h-b$.

4) Apply the Pythagorean Theorem, i.e., $\overline{AB'}^2 = d^2 + (2h-a-b)^2$.

As following above steps, we calculated the distance of simple cases in Figure 3.3 and complex cases in Figure 3.4. In addition, we found the general equation as Figure 3.5. In such general equation, the major factor is n_{sp}, i.e., the number of reflection times on the sea surface. As increasing n_{sp}, infinitely many paths can be generated but we only considered paths within a 30 dB energy gap against the direct path. There exist over than 8 rays in such limitation, which is enough to cover channel characteristic of shallow underwater [16].

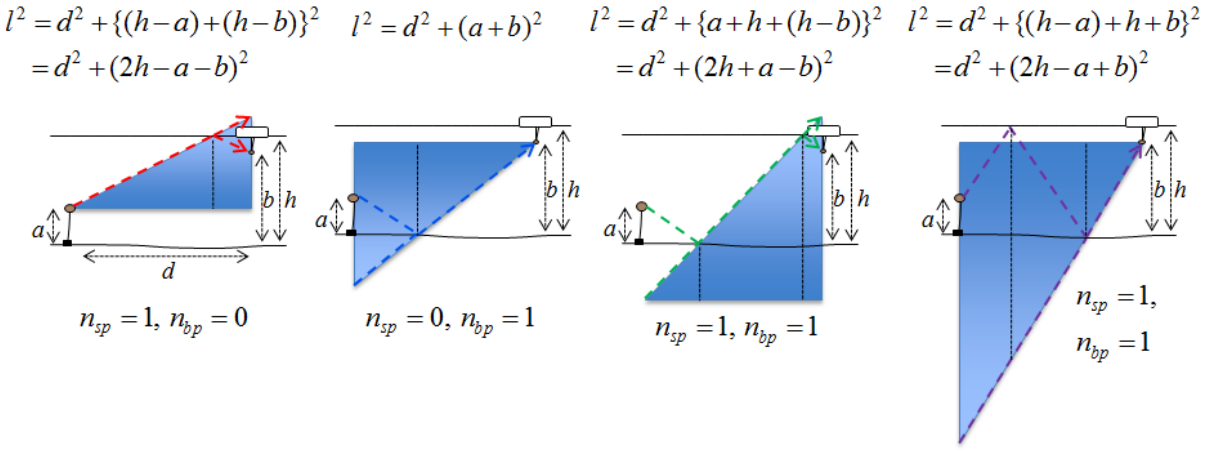

Figure 3.3 Simple cases of reflection path

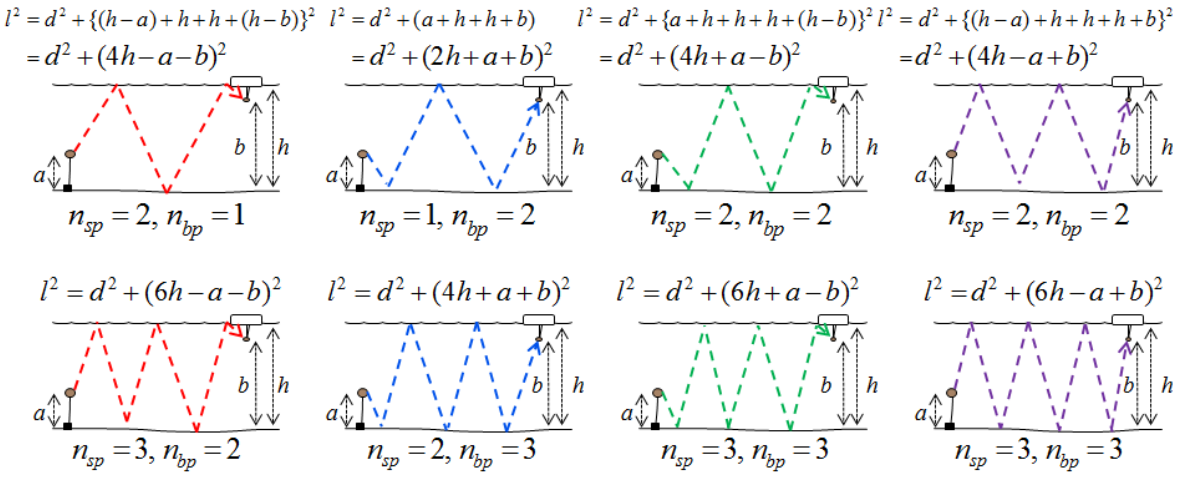

Figure 3.4 Complex cases of reflection path

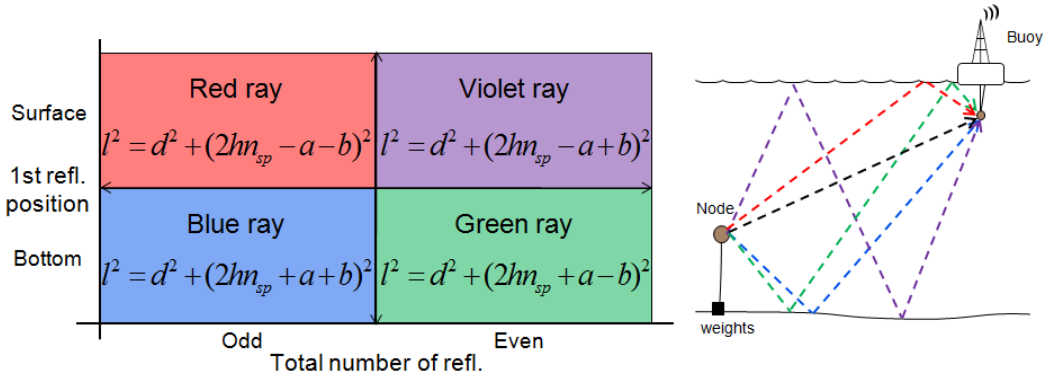

Figure 3.5 General equation of reflection path

3.1.3 Simulation Channel Analysis

We generated multipath with considering reflection characteristics and obtained impulse response about simulation channel as shown in Figure 3.6 and Figure 3.7. We set the maximum delay spread as 25 ms, since there is no tap over about 25 ms in Figure 3.7. Thus, coherence bandwidth as 40 Hz since these is in the reciprocal number relation.

Moreover, we verified the limited creation of multipath according to position of node and buoy, though Figure 3.8. Since there are too many possible combinations of node and buoy depth, we chose the special cases only that are mentioned section 2.5.

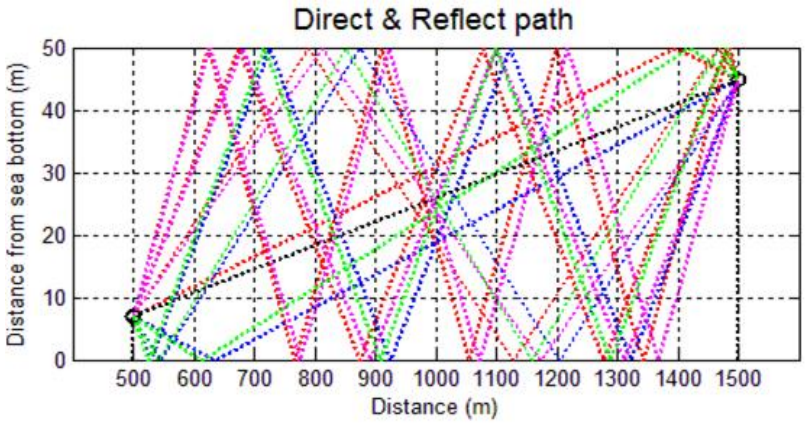

Figure 3.6 Multipath of simulation channel

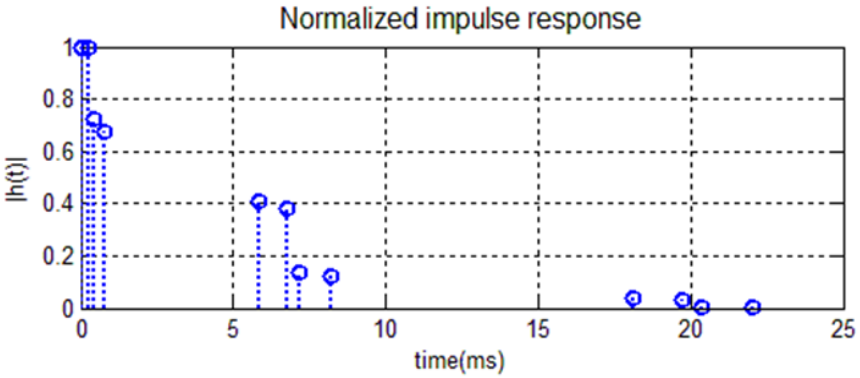

Figure 3.7 Impulse response of simulation channel (Original case)

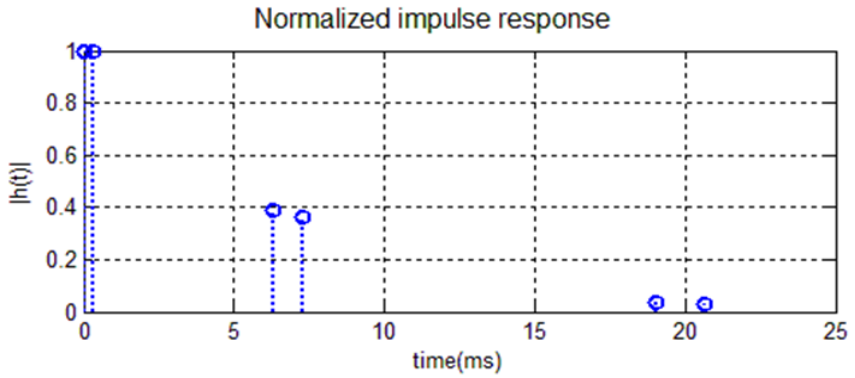

(a) Node is located on ocean bottom

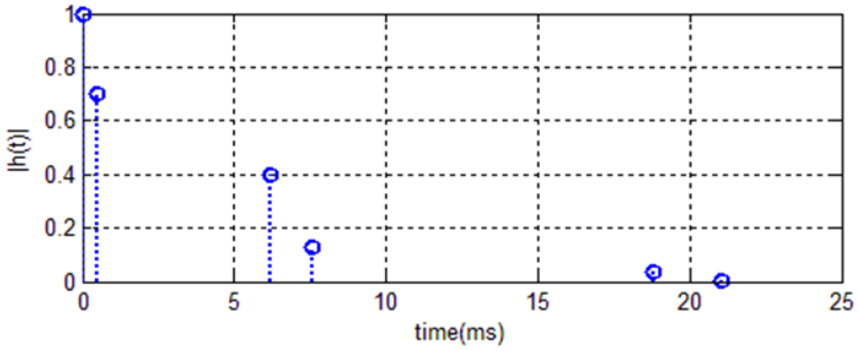

(b) Buoy is located on sea surface

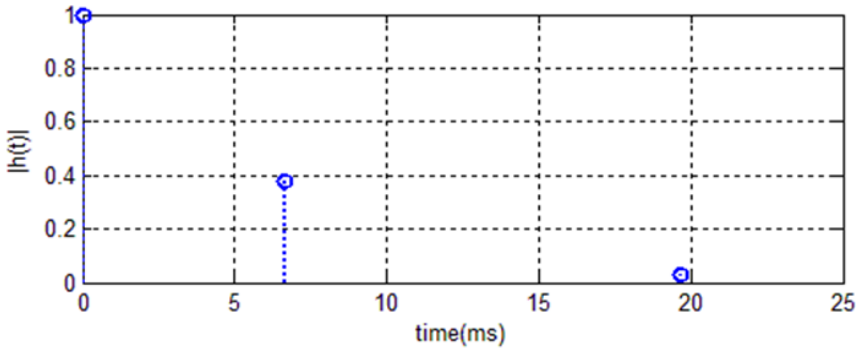

(c) Node is located on ocean bottom & Buoy is located on sea surface

Figure 3.8 Impulse response of simulation channel (Special cases)

3.2 OFDM System Design

3.2.1 OFDM System over UAC

In the special case that time variation of the channel is sufficiently slower than the symbol rate, the frequency selective fading is surmountable via OFDM system [18]. To overcome frequency selective fading, the sub-carrier bandwidth should be smaller than the coherent bandwidth of the channel. In addition, to solve ISI, a guard period that is larger than the maximum delay spread should be inserted between the connected symbols. The back part of a valid symbol is copied and inserted as the cyclic prefix (CP) [19]. Furthermore, to deal with time selective fading, the OFDM symbol duration should be substantially smaller than the coherent time of the channel [20].

For OFDM systems, it is known that deep fading at certain specific sub-carriers is detrimental to system performance. To mitigate this negative effect, error correction codes such as convolution codes, Reed-Solomon codes, turbo codes, and LDPC codes are usually used [18][9].

Under OFDM systems operating over UAC, the Doppler spread comes from the drift of the node and buoy can easily destroy orthogonality. Moreover, a long guard period is needed, since the relatively slow propagation speed (in RF channel $\approx 3\times 10^{8}$ m/s, in UAC $\approx 1,500$ m/s) causes a large maximum delay spread.

There have been approaches to solve this orthogonality destruction problem caused by the frequency offset. The authors in [21] suggested using the orthogonal matching pursuit (OMP) algorithm based on the channel estimation. Other approaches include adaptive phase synchronization on the time domain [22] and adaptive OFDM signal detection algorithm [23]. However, the application of such system designs that depend on synchronization and frequency offset equalization is limited because of its high complexity. In this section we circumvent this problem by selecting the OFDM system parameters carefully.

3.2.2 System Block Diagram

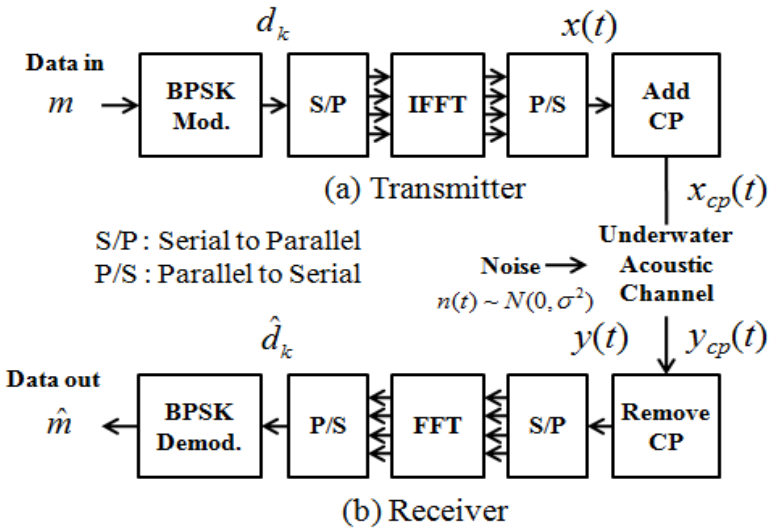

Figure 3.9 Block diagram of OFDM system

Figure 3.9 is a block diagram of the OFDM system through UAC. The input data sequence m is assigned to each sub-carrier after binary phase shift keying (BPSK) modulation. Such assigned sequence d_k is transmitted through UAC in time domain after inverse fast Fourier transform (IFFT) processing and CP period addition.

$$d_k = 2m_k - 1 \tag{3.1}$$

$$x(t) = \mathrm{IFFT}\{d_k\} \tag{3.2}$$

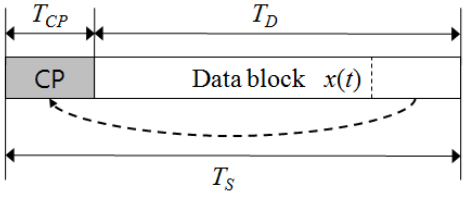

Figure 3.10 Generation of x_{cp}

$$y_{cp}(t) = h(t) * x_{cp}(t) + n(t),\ n(t) \sim N(0, \sigma^2) \tag{3.3}$$

After removing CP period, the received digital signal on frequency domain is obtained via and FFT processing of $y_{cp}(t)$ as follows.

$$Y[k] = H[k]d_k + N[k], \tag{3.4}$$

where $H[k]$ and $N[k]$ are FFT results of impulse response and Gaussian noise, respectively.

The equalized signal $\hat{d}_k$ is

$$\hat{d}_k = \Re eal\left\{\frac{Y[k]}{\hat{H}[k]}\right\}, \tag{3.5}$$

where $\hat{H}[k]$ is estimated channel transfer function. In this paper, we assume perfect channel estimation, i.e., $\hat{H}[k]$ is exactly the same with $H[k]$. Consequently, $\hat{d}_k$ is represented as

$$\hat{d}_k = d_k + n'_k,\ \ n'_k \sim N(0, \tilde{\sigma}^2 = \frac{\sigma^2}{H^2[k]}). \tag{3.6}$$

.

3.2.3 OFDM System Parameter Setting

Table 3.1 represents the suggested coded OFDM system parameters. As we mentioned above in section 2.3, since Doppler spread increases geometrically, as the carrier frequency increases, to overcome time selective fading, we should select a carrier frequency that is as low as possible. However, the use of a too low carrier frequency causes a limitation of the available transmission bandwidth. In this paper, we chose a 7 kHz carrier frequency assuming the use of 10 kHz bandwidth. Such bandwidth is based on typical bandwidths of UAC for different ranges. Since we modeled distance as 1,000 m, i.e., *medium* range, approximately 10 kHz bandwidth is suitable to system [24].

In addition, to overcome the ISI problem, we set the CP period as 25 ms via analysis of impulse response of modeled channel. Under this setting, the maximum delay spread and coherent time of the channel are about 4.744 Hz and 210 ms, respectively.

It is essential to choose a number of sub-carriers that satisfy conditions to overcome frequency selective fading $(\Delta f \le B_C)$ and time selective fading $(T_S \ll T_C)$ to deal with both problems at the same time. In this paper, we chose 256 sub-carriers to satisfy these conditions. Consequently, the OFDM symbol duration, i.e., summation of valid symbol duration and CP period, is 50.6 ms

The suggested OFDM is able to overcome not only frequency selective fading, since the sub-carrier bandwidth (39.0625 Hz) is smaller than coherent bandwidth of channel (40 Hz); but also ISI, since CP period (25 ms) is larger or equal than maximum delay spread; as well as time selective fading, since the OFDM symbol duration (50.6 ms) is sufficiently smaller than coherent time of channel (210 ms).

Table 3.1 OFDM system parameters

Parameter	Value
Carrier frequency	7 kHz
Transmission bandwidth : BW	10 kHz
Maximum Doppler Spread : $B\tau_{max}$	4.744 Hz
Coherent Time : $T_C = 1/ B\tau_{max}$	210 ms
Maximum Delay Spread : τ_{max}	25 ms
Coherent Bandwidth : $B_C=1/\tau_{max}$	40 Hz
Number of sub-carriers : N_{FFT}	256
Sub-carrier bandwidth : $\Delta f = BW/N_{FFT}$	39.0625 Hz
Valid symbol duration : $T_D = 1/\Delta f$	25.6 ms
CP period : $T_{CP} \ge \tau_{max}$	25 ms
OFDM symbol duration : $T_S = T_D+T_{CP}$	50.6 ms

Table 3.2 OFDM parameter setting table

OFDM system parameter	Equation		Value	
Transmission Frequency Band	=B4-B3/2	=B4+B3/2	2000	12000
Transmission bandwidth BW			10000	
Center frequency			7000	
Maximum Doppler Spread $B\tau max$	Wind speed	15	Wind speed	15
	=(0.0175/1500)*B4*(C5^(3/2))		4.744404599	
Coherent Time $1/B\tau max$	=1/B6		0.210774604	
Maximum Delay Spread τmax			0.025	
Coherent Bandwidth Bc = 1/ τmax	=1/B8		40	
FFT size N_{FFT}			256	
Sub-carrier Frequency $\triangle f = BW/N_{FFT}$	=B3/B10	=IF(B11<=B9,"Satisfaction","Dissatisfaction")	39.0625	Satisfaction
Origianl OFDM symbol duration T_D=1/$\triangle f$	=1/B11		0.0256	
CP time $T_{CP} \geq \tau max$	=B8		0.025	
OFDM symbol duration $T_s = T_D + T_{CP}$	=B12+B13	=IF(B14<=(B7/4),"Satisfaction","Dissatisfaction")	0.0506	Satisfaction

Table 3.2 shows the Excel sheet used in process of finding parameters to satisfy above conditions.

1) First of all, we filled the maximum delay spread as 0.025, thus CP time set as 0.025 and coherent bandwidth as 40, naturally. This figure is based on Figure 3.7.

2) As a next step, we filled the transmission bandwidth as 10,000 based on typical value in [24] and chose the center frequency as low as possible with considering transmission frequency band. After filling, maximum Doppler spread and coherent time are calculated, automatically.

3) Finally, we selected the size of FFT. The size is suitable that makes two ‘Satisfaction’ in sub-carrier frequency row and OFDM symbol duration row. ‘Satisfaction’ in sub-carrier frequency row is about frequency selective fading and other is about time selective fading. After selecting this figure, others (i.e., sub-carrier frequency, original OFDM symbol duration and OFDM symbol duration) are calculated, automatically.

   In case of ‘Dissatisfaction’ in OFDM symbol duration row, FFT size or center frequency should be decrease. On the other hand, in case of ‘Dissatisfaction’ in sub-carrier frequency row, bandwidth should be decrease or FFT size should be increase.

3.2.4 Performance Verification

As mentioned above section, deep fading at certain specific sub-carriers is detrimental to system performance. In addition, a long guard period cause energy efficiency decline. In such reason, bit-error-rate (BER) performance of system designed so far is not good as shown Figure 3.11. Although such system obtained 10^{-3} BER performance at the 23 dB SNR, it is not enough robust since the battery power is limited. Further, Figure 3.12 and Figure 3.13 show the wide performance variation according to channel change. Such results cannot assure the robust performance since there is possibility that is position changing of node and buoy in realistic system. Thus, we combined LDPC code to mitigate this negative effect.

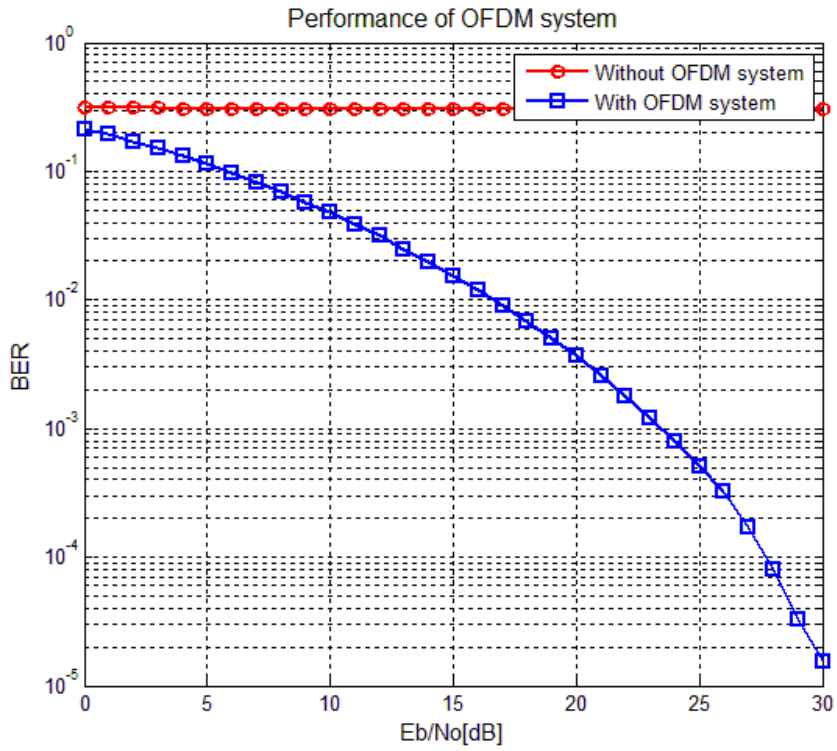

Figure 3.11 Performance of ODFM system (D_T= 7 m, D_R= 45 m)

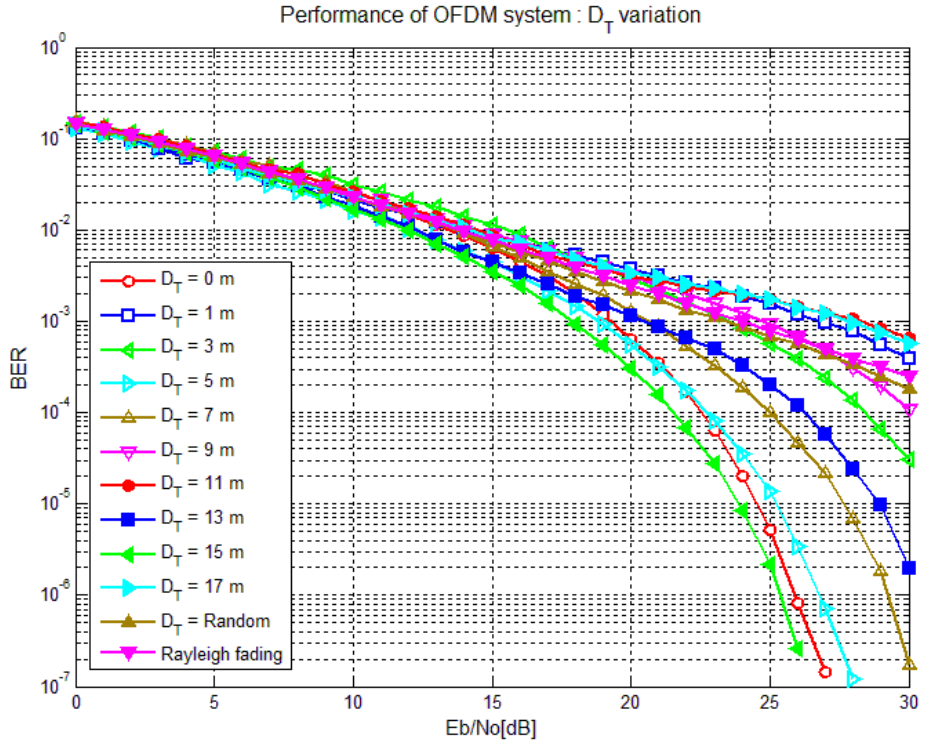

Figure 3.12 Performance of ODFM system (D_T variation case, D_R = 45 m)

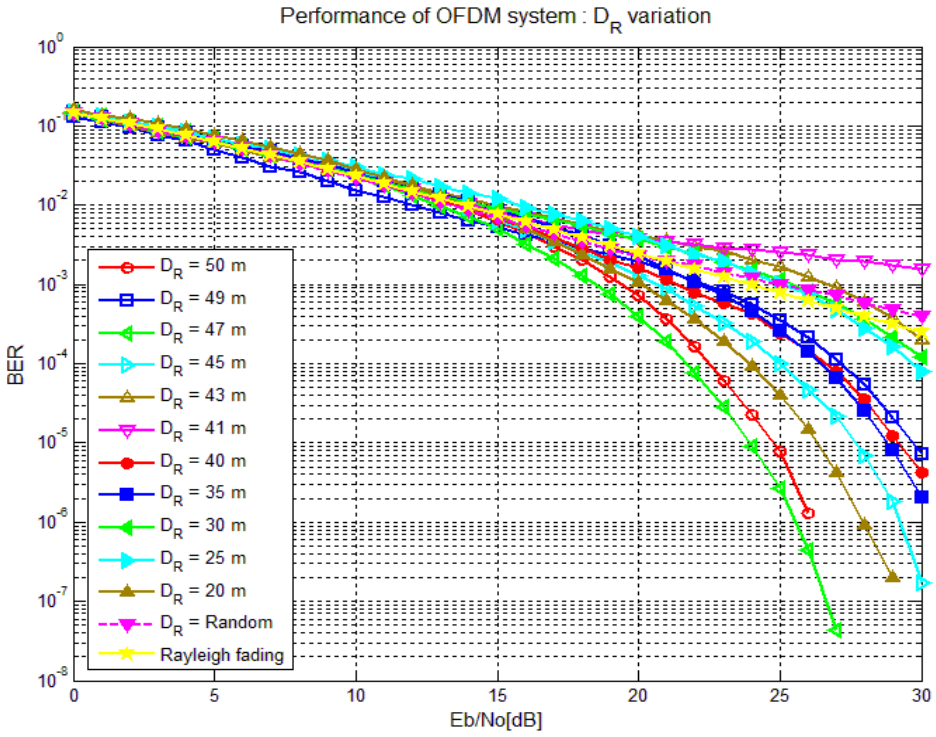

Figure 3.13 Performance of ODFM system (D_T= 7 m, D_R variation case)

3.3 LDPC coded OFDM System Design

3.3.1 LDPC code

The LDPC codes used in this paper were suggested by R. G. Gallager in 1962 and known as one of the most advanced error correction codes. The parity check matrix H of the LDPC codes consists of numerous zeroes and only a few ones in a kind of sparse matrix. Commonly, regular LDPC codes are represented as (n, j, k) where n is block length and j and k are the number of ones on each row and column of the parity check matrix, respectively [25][26].

In this paper, we generated a regular LDPC code via following process.

1) Pseudo random matrix H_{pseudo} is constructed by k times repetition of identity matrix H_{seed} with size n/k by n/k.

$$H_{seed} = I_{n/k \text{ by } n/k} \tag{3.7}$$

$$H_{pseudo} = [\underbrace{H_{seed} \quad H_{seed} \quad \cdots \quad H_{seed} \quad H_{seed}}_{k \text{ times}}] \tag{3.8}$$

2) Parity check matrix H is constructed by L times column permutation of H_{pseudo} matrix where $L = (n/k)\,?j$ is the number of check node.

$$H = \begin{bmatrix} H_{pseudo} \\ \text{permutated } H_{pseudo} \\ \vdots \\ \text{permutated } H_{pseudo} \end{bmatrix} \Big\} L \text{ times} \tag{3.9}$$

3) Systematic parity check matrix $H_{sys} = [I \mid P]$ is constructed by Gaussian elimination of parity check matrix H, and then is used to construct generator matrix $G_{sys} = [P^{\mathrm{T}} \mid I]$.

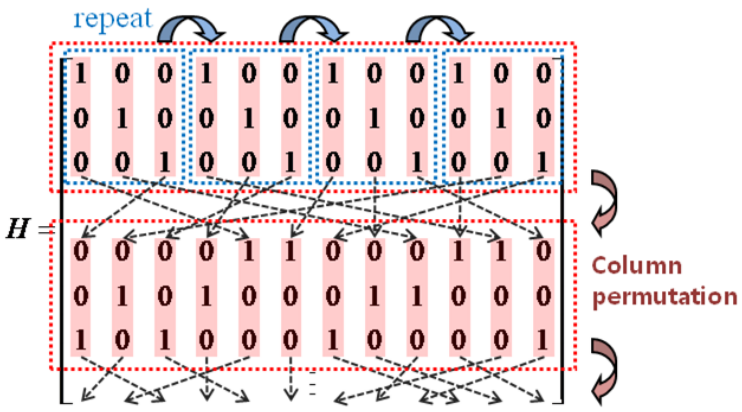

Figure 3.14 The parity check matrix generation concept

Figure 3.14 represents the concept of the parity check matrix H construction process via column permutation of the pseudo random matrix H_{pseudo}.

3.3.2 System Block Diagram

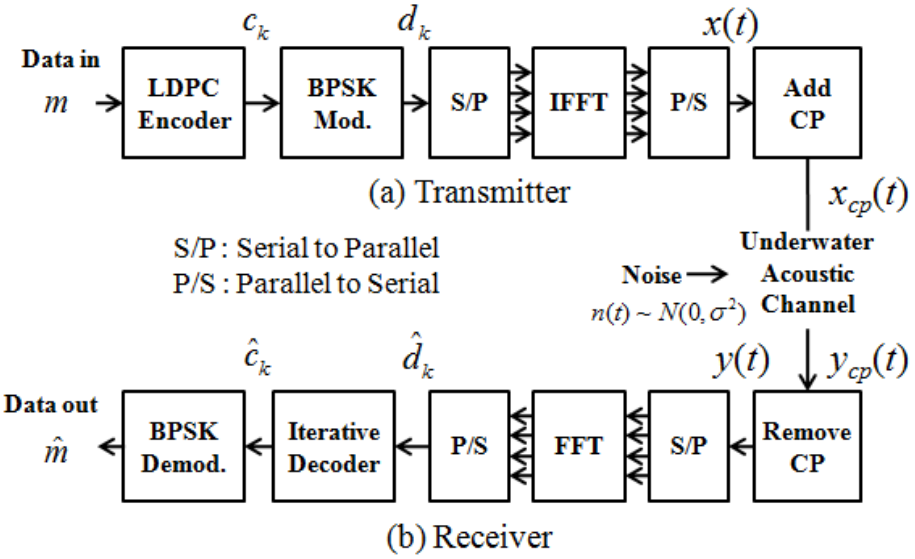

Figure 3.15 Block diagram of LDPC coded OFDM system

Figure 3.15 is a block diagram of the suggested coded OFDM system using the regular LDPC code. The input data sequence *m* is multiplied with generator matrix G_{sys} of the LDPC code, and then constructs c_k. After BPSK modulation, c_k is assigned to each sub-carrier.

$$\mathbf{c}_k = \mathbf{mG_{sys}},\ k = 1, 2, \cdots, n \tag{3.10}$$

$$d_k = 2c_k - 1 \tag{3.11}$$

Others are exactly same with procedure of OFDM system explained in above section 3.2 except the iterative decoder. The equalized signal $\hat{d}_k$ is used to set the initial log likelihood ratio (LLR) values at the iterative decoder. The iterative decoder gradually renews LLR values via message passing between bit nodes and check nodes. The LLR message passing algorithm is as follows [27].

1) The initial LLR value is set by using equalized signal $\hat{d}_k$.

2) The iteration processes are divided in two, the bit-to-check message process and the check-to-bit message process. The Q1 matrix represents connections from bit nodes to check nodes having a size of m by t, where m and t are connection order and bit node index, respectively, i.e., $\mathrm{Q1}(m, t)$ signify check node index having m-th connection from t-th bit node. As an example, assuming the 1st bit node has a connection with the 3rd and 5th check nodes and the 2nd bit node has a connection with the 1st and 7th check nodes, the Q1 matrix is

$$\mathbf{Q1} = \begin{bmatrix} 3 & 1 \\ 5 & 7 \end{bmatrix}. \tag{3.12}$$

Similarly, the Q2 matrix represents connections from check nodes to bit nodes having a size of m by l, where m and l are the connection order and check node index, respectively, i.e., $\mathrm{Q2}(m, l)$ denotes a bit node index having m-th connection from the l-th check node.

The iterative decoder repeats this bit-to-check message process and check-to-bit message process every iteration time. In this paper, we repeated such bit-to-check message process and check-to-bit message process 20 times.

3) After all iterations, the iterative decoder calculates the final LLR values.

4) The $\hat{d}_k$ is decided through decision part.

Table 3.3 LLR message passing algorithm

1) Initialize

- $LR(\mathrm{f}_t) = \frac{2}{\tilde{\sigma}^2}\hat{d}_k = \frac{2H^2[k]}{\sigma^2}\hat{d}_k = \frac{4E_sH^2[k]}{N_o}\hat{d}_k$

- $LR(\mathrm{r}_{tl}) = 0$, $t = 1, 2, \cdots, n$ and $l = 1, 2, \cdots, k$

2) Iteration

- Bit-to-Check messages:

  $LR(\mathrm{q}_{t,Q1(m,t)}) = LR(\mathrm{f}_t) + \sum_{m' \neq m} LR(\mathrm{r}_{t,Q1(m',t)})$, where $t = 1, 2, \cdots, n$ and $m = 1, 2, \cdots, j$

- Check-to-Bit messages:

  $LR(\mathrm{r}_{Q2(m,l),l}) = \prod_{m' \neq m} \mathrm{sgn}(LR(\mathrm{q}_{Q2(m',l),l})) \times f[\sum_{m' \neq m} f(|\, LR(\mathrm{q}_{Q2(m',l),l})\,|)](-1)^k$,

  where $l = 1, 2, \cdots, L$, $m = 1, 2, \cdots, k$ and $f(x) := -\log(\tanh(x/2)) = \log[(e^x + 1)/(e^x - 1)]$

3) Output

- $LR(\mathrm{p}_t) = LR(\mathrm{f}_t) + \sum_m LR(\mathrm{r}_{t,Q1(m,t)})$

4) Decision

- *if* $LR(\mathrm{p}_t) > 0$, $\hat{c}_t = 1$; *else* $\hat{c}_t = -1$

3.3.3 LDPC code Parameter Setting

Table 3.4 LDPC code parameters

Parameter	Value
Type	*Regular*
Block size : n	256
# of 1s in a column : j	4
# of 1s in a row : k	8

When designing the LDPC code, as the j and k parameters increase, the minimum distance of the codes increase but we cannot guarantee the work of the iterative decoder since the parity check matrix is too dense. Thus, we consider this trade-off relationship and set the parameters of j and k to 4 and 8, respectively, i.e., rate half code. Further, we set block size n to 256. These are the same as the number of sub-carriers to combine with the previously designed OFDM system.

3.3.4 Performance Verification

Figure 3.16 shows the BER performance of the suggested OFDM system. These result shows the overcoming of the performance falloff via the LDPC coded OFDM system. In detail, over a certain threshold of received SNR, this system is able to solve the performance falloff problem caused by deep fading at certain specific sub-carriers. To be specific, this system not only achieved a 17 dB SNR benefit, but also reduced the SNR variation, according to channels. Such reduction of the SNR variations is shown in the Figure 3.17 and Figure 3.18. As combining LDPC codes and OFDM system, the performance variation reduced noticeably from about 10 dB to 3 dB at the 10^{-3} BER point versus the un-coded OFDM system. These results mean assuring robust performance even the positions of node and buoy are changed in the realistic channel.

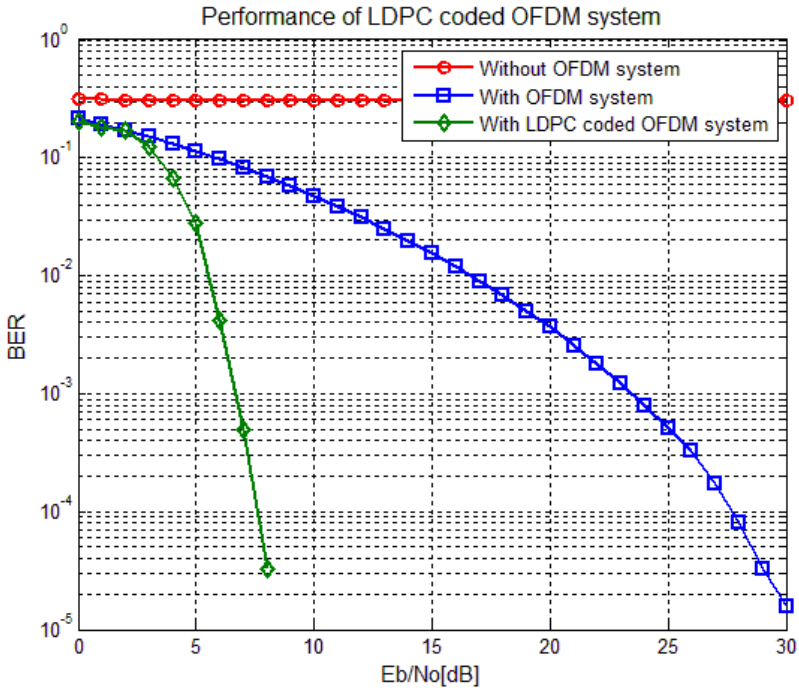

Figure 3.16 Performance of LDPC coded ODFM system (D_T = 7 m, D_R = 45 m)

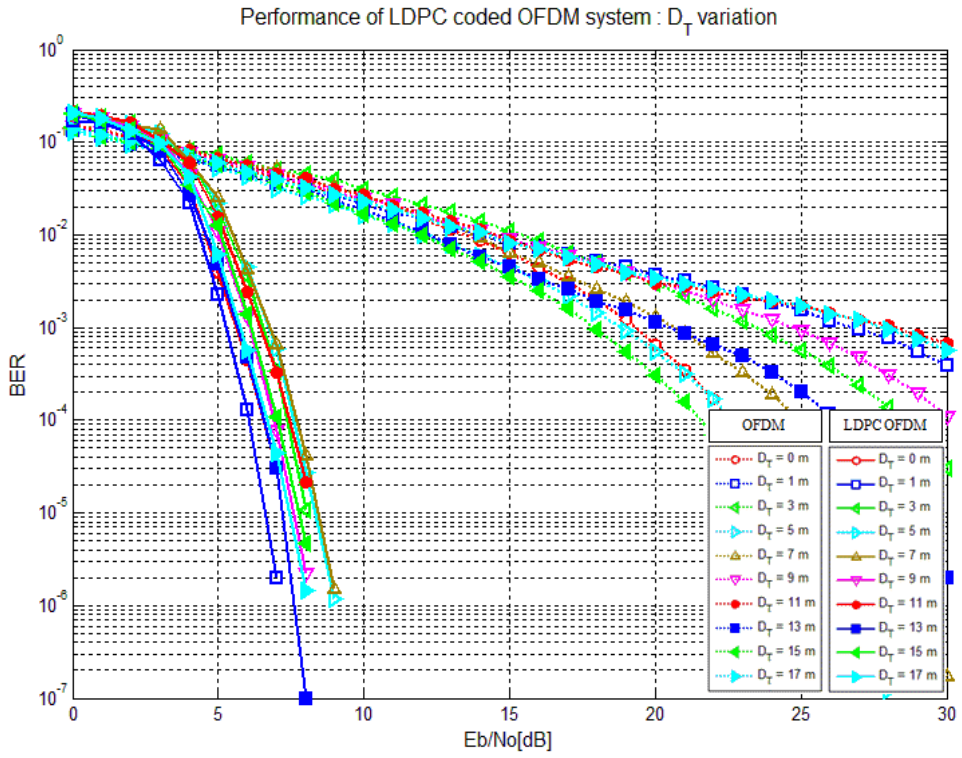

Figure 3.17 Performance of LDPC coded ODFM system (D_T variation case, D_R = 45 m)

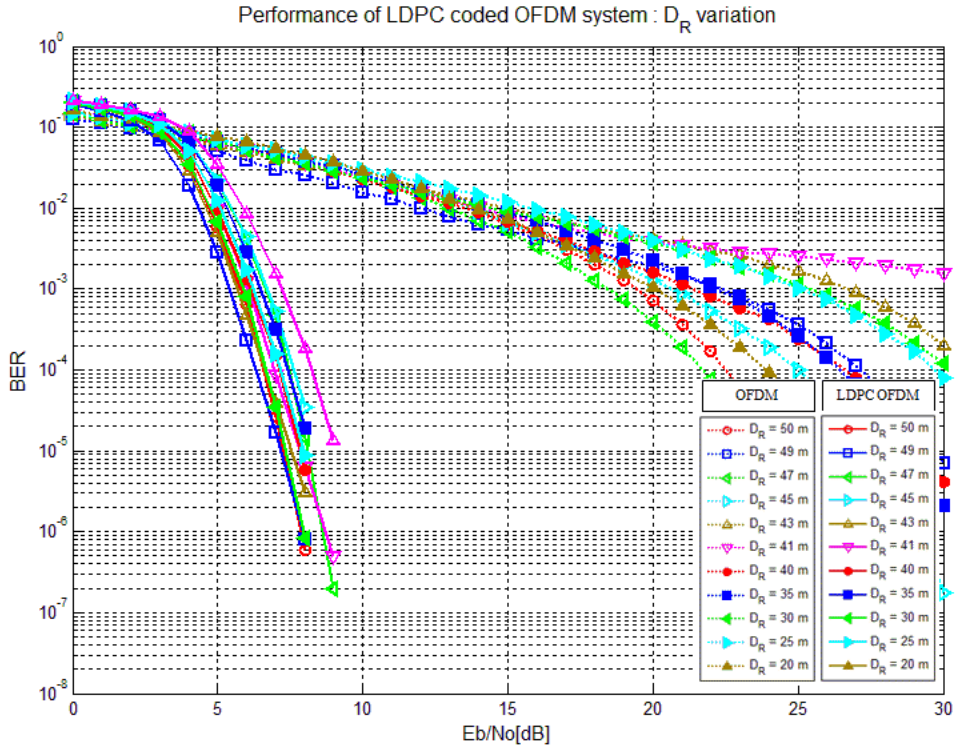

Figure 3.18 Performance of LDPC coded ODFM system (D_T= 7 m, D_R variation case)

3.4 Results and Discussion

Until now, we have suggested the LDPC coded OFDM system as one of solution to obtain robust performance in UAC. However, there are some problems to apply to realistic system. Since underwater sensors are able to failure due to fouling and corrosion, as well as discharge due to limited battery power, such peer-to-peer communication system cannot assure the working of the system. Further, we have assumed the almost flat condition of sea surface and ocean bottom so far, but this assumption is not fit perfectly to realistic system. Although the channel looks as if that is ideally flat in wide vision, there are some rocks, coral reef, pebbles, cracks, slopes, etc. in small vision. These cause fading effect. Thus, we modeled such fading effect as lognormal random distribution [28]. Figure 3.19 denotes the lognormal random distribution with mean 1 and variance 2.

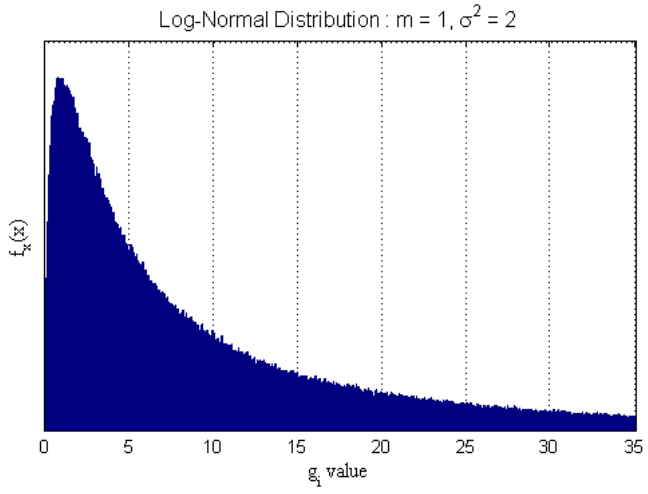

Figure 3.19 Lognormal distribution (m = 1, σ^2 = 2)

In lognormal random distribution model, we multiplied such channel gain coefficient g_i, i.e., following lognormal random distribution with mean 1 and variance 2 in (3.3) as follows.

$$y_{cp}(t) = g_i\, h(t) * x_{cp}(t) + n(t),\ \ n(t) \sim N(0, \sigma^2)\,, \tag{3.13}$$

where g_i, $i = 0, 1, 2, \cdots$ is fixed while OFDM symbol duration time. Actually, each tap of impulse response should have designed as lognormal random distribution individually, but we assumed the same channel gain within a symbol transmission to reduce the complexity.

Figure 3.20 denotes the performance falloff of un-coded OFDM system and LDPC coded OFDM system, according to lognormal fading. Although we used the LDPC code to mitigate negative deep fading effect at certain specific sub-carriers, we need about 18 dB SNR to obtain 10^{-3} BER performance, which is not enough robust either. User cooperation have been particularly beneficial for such fading wireless systems, since while an individual channel operating alone may be useless due to severe path loss or deep channel fading, combined together a set of channels may become useful again. Thus, we tried to overcome such fading effect via user cooperation based on LDGM codes. In the next section, we discussed LDGM-LDPC concatenated coded OFDM system on multiple sensor networks.

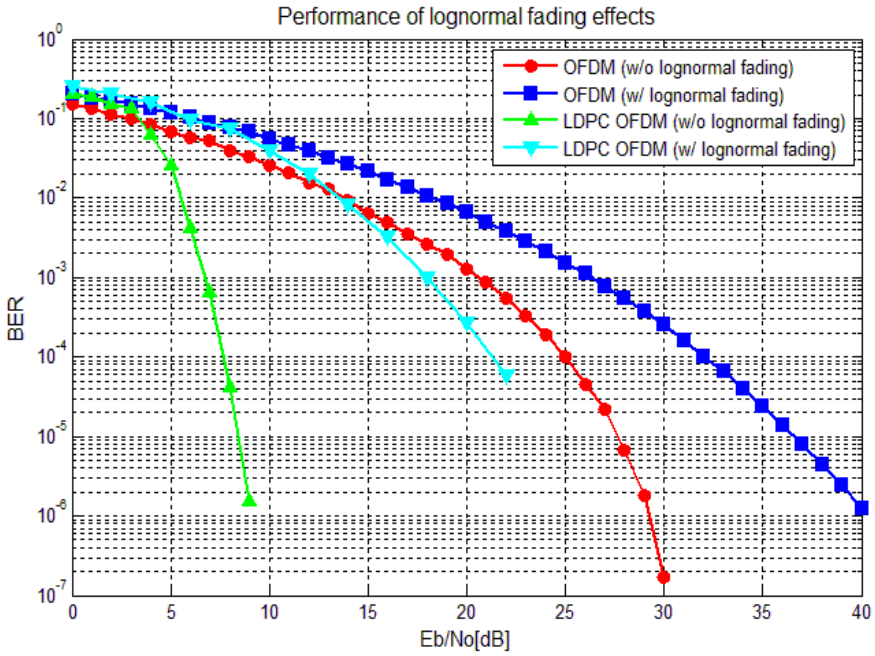

Figure 3.20 Performance of lognormal fading effects

4 Multiple Sensor Networks Design

4.1 Simulation Channel Model

4.1.1 Ideal model (Non-lognormal fading channel)

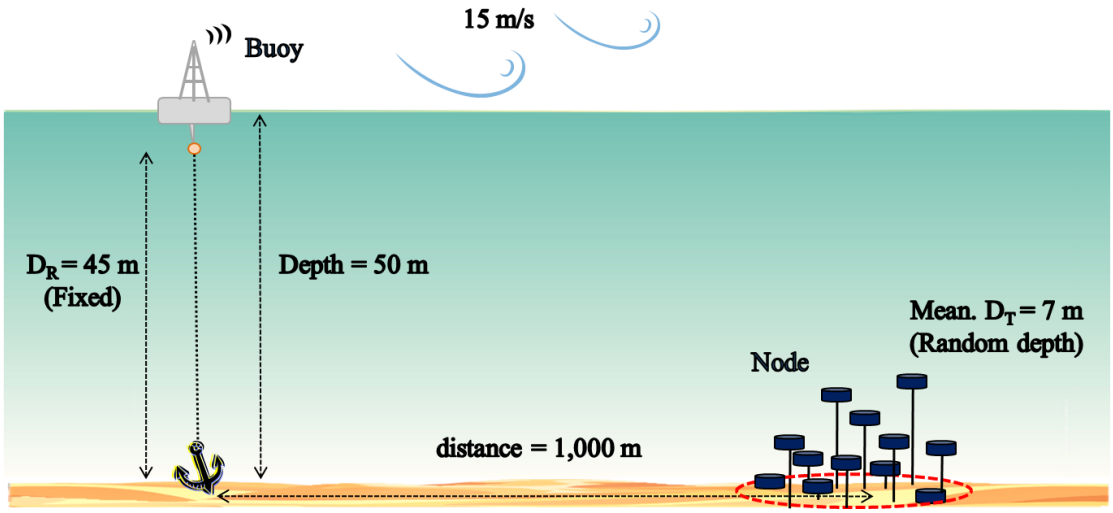

Figure 4.1 Ideal simulation channel model (Non-lognormal fading)

In this section, the simulation channel is modeled for multiple sensor networks under the ideal condition, i.e., having almost flat condition on sea surface and ocean bottom as shown in Figure 4.1. The major difference of such model against previous model is the number of sensor nodes. In this paper, we assumed the number of sensor nodes as [10, 30, 50, 100], which are at averagely 7 m from the ocean bottom within some limited range (Red dashed line in Figure 4.1). For our simulation, we generated the depth and position randomly for every OFDM symbol, channels responses between the nodes and buoy are changed all the time. However, such random generation is limited to nodes only. In case of buoy, it is fixed as 5 m. Other factors are exactly same with previous simulation channel model; a maximum sea surface wind speed is 15 m/s, water depth is 50 m, distance between the node and buoy is 1,000 m.

4.1.2 Realistic model (Lognormal fading channel)

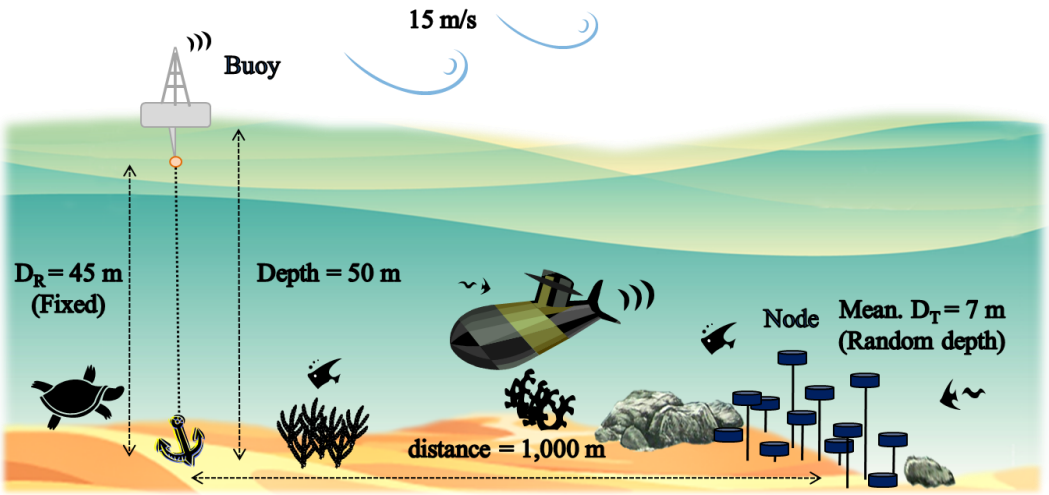

Figure 4.2 Realistic simulation channel model (Lognormal fading)

As we have said above section 3.4, there are possibilities in realistic UAC, i.e., occurrence of shadow fading caused by some materials and natural environment like submarine, rock, coral reef, pebble, crack, slope, fish, ocean mammal, etc. and failure in sensor node. The failure in sensor node can be represented as other meaning, i.e., channel gain is equal to zero. Since lognormal random variable contains zero value, such shadow fading and failure can be modeled as a lognormal random distribution.

To show the system performance over realistic channel, we used not only ideal model, i.e., non-lognormal fading channel, but also realistic model designed as a lognormal random distribution with mean 1 and variance 2.

4.2 LDGM-LDPC concatenated OFDM System Design

4.2.1 LDGM code

Whereas channel coding has long been established as a fundamental technology for protecting bit streams error caused by noise and fading, network coding has only recently found. Among the existing studies that exploit network coding in user cooperation, one work that proposes *adaptive network coded cooperation* (ANCC) is particularly outstanding [29].

The LDGM code is a special class of linear-time encodable LDPC codes. The parity check matrix of a systematic LDGM code consists of two parts, a sparse (and random) matrix P on the left and an identity matrix I on the right as shown Figure 4.3.

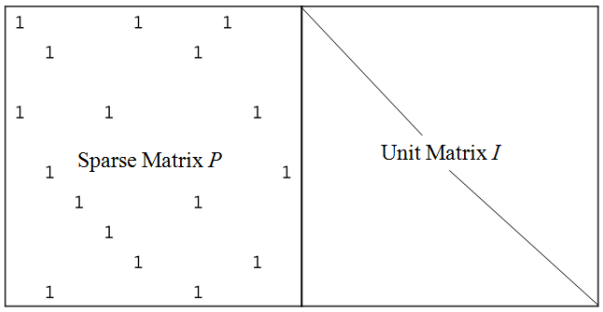

Figure 4.3 The parity check matrix of LDGM code

The model of interest here comprises m nodes communicating wirelessly to a common destination via two-phase user cooperation. In each phase, the m nodes transmit binary phase-shift keying (BPSK) modulated data through time division multiple access (TDMA). We assume that all the communication channels used in this paper are spatially independent. Without loss of generality, we consider that each channel follows a frequency nonselective slow fading.

The ANCC protocol proposed in [29] proceeds as follows.

1) First phase : Broadcast phase

Each node broadcasts its data packet of length N in its assigned time slot gradually. Except the transmitting node in own turn, other nodes listen and try to decode what it hears. Actually, due to channel condition and other interference, a node may not be able to receive all other source packets. We use receive-set, $\mathrm{R}(i)$, to denote the set of packets that node i decoded correctly, where $\mathrm{R}(i) \subset \{1, 2, \cdots, m\}$.

2) Second phase : Relay phase

Each node randomly selects a small number of packets from its receive-set, computes their checksum and forwards the length-N check-sum packet to the destination in its assigned time slot. Meanwhile, those nodes that have not yet had a chance to relay continue to listen and decode. The correctly received relay-packets will continue to be included in the decode-set $\mathrm{R}(i)$. Since the system operates in a TDMA manner, the decode-set satisfies $\mathrm{R}(i) \subset \{1, 2, \cdots, m\}$. Hence, by the end of the second phase, the *m* nodes have transmitted, through user cooperation, a $(2m, m)$ network code in the form of a randomly systematic LDGM code.

The source-packets transmitted in the first phase constitute the systematic symbols of the network code, and the relay-packets transmitted in the second phase constitute the parity symbols.

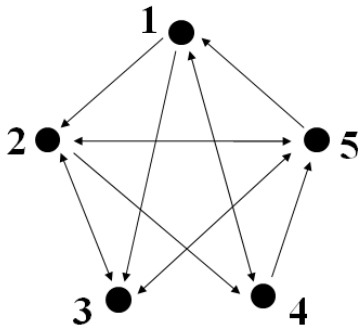

Figure 4.4 An example of 5 nodes sending data to a common destination

To illustrate, consider a simple example of $m=5$ nodes. Assume that for a particular period of cooperation, the inter-user channels form an instantaneous network topology as shown in Figure 4.4, where a directed link represents a quality connection that lasts throughout this period of cooperation. The receive-set of each node contains, respectively,

$$\mathrm{R}(1)=\{\mathbf{1},\mathbf{4},\mathbf{5}\},\ \mathrm{R}(2)=\{1,\mathbf{2},\mathbf{3},\mathbf{5}\},\ \mathrm{R}(3)=\{\mathbf{1},2,\mathbf{3},\mathbf{5}\},\ \mathrm{R}(4)=\{\mathbf{1},\mathbf{2},\mathbf{4}\},\ \mathrm{R}(5)=\{\mathbf{2},\mathbf{3},\mathbf{4},5\}$$

Assuming that the packets marked in bold font are selected (randomly) by each terminal to form check sums, add the selected packets together, we obtain a parity check matrix of the resulting network code:

$$H=\left[\begin{array}{ccccc|ccccc} \overbrace{1}^{} & \overbrace{2}^{} & \overbrace{3}^{} & \overbrace{4}^{} & \overbrace{5}^{} & \overbrace{6}^{} & \overbrace{7}^{} & \overbrace{8}^{} & \overbrace{9}^{} & \overbrace{10}^{} \\ 1 & 0 & 0 & 1 & 1 & 1 & 0 & 0 & 0 & 0 \\ 0 & 1 & 1 & 0 & 1 & 0 & 1 & 0 & 0 & 0 \\ 1 & 0 & 1 & 0 & 1 & 0 & 0 & 1 & 0 & 0 \\ 1 & 1 & 0 & 1 & 0 & 0 & 0 & 0 & 1 & 0 \\ 0 & 1 & 1 & 1 & 0 & 0 & 0 & 0 & 0 & 1 \\ \underbrace{}_{\text{systematic symbols}} & & & & & \underbrace{}_{\text{parity symbols}} & & & & \end{array}\right] \tag{3.14}$$

Due to the random formation of the code, a small bit-map field needs to be included in the relay-packet, so that the destination knows how the checks are constructed and can correspondingly replicate the code graph and perform message passing decoding.

4.2.2 LDGM-LDPC concatenated OFDM System

Since we have used LDPC coded OFDM system for peer-to-peer communication, each node broadcasts not bit stream data but OFDM symbol coded as LDPC code in frequency domain. Thus, each node needs time to decode OFDM symbol and re-encode OFDM symbol, as well as time to listen. Consequently, we obtained codeword that coded in spacial domain, as well as time domain as shown Figure 4.5. This codeword is rate one fourth since we used rate half LDPC code in frequency domain and rate half LDGM code in spacial domain.

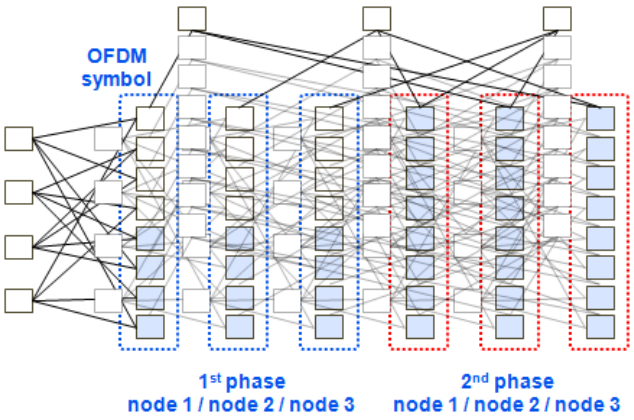

Figure 4.5 Graph of LDPC-LDGM code

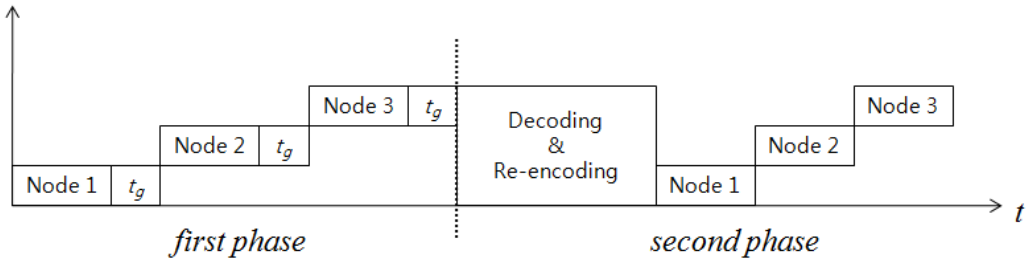

Figure 4.6 Sequence of transmission

Figure 4.5 and Figure 4.6 are simple example having 3 nodes cooperation. Each node transmitted LDPC coded OFDM symbol in regular sequence. In this paper, we assumed that each node is able to receive and recovery all OFDM symbols from others nodes, thus the guard time t_g is needed to overcome difference of arrival time. After first phase, each node knows what other nodes send. At the second phase, each node decodes received OFDM symbol and re-encodes OFDM symbol by using LDGM parity check matrix. Since LDPC-LDGM coded OFDM symbol is transmitted to not nodes but buoy, the difference of arrival time between each node and buoy is almost same. Because of such reason, the system doesn't need additional guard time like as t_g.

In the assuming each node is able to receive and recovery all OFDM symbols from others nodes, as increase the range of distributed nodes, t_g should be increase, which is another trade-off relationship. As increase the range of distributed nodes, we can obtain bigger effects of spacial domain diversity. However, there is a disadvantage, i.e., t_g should be increase.

4.2.3 System Block Diagram

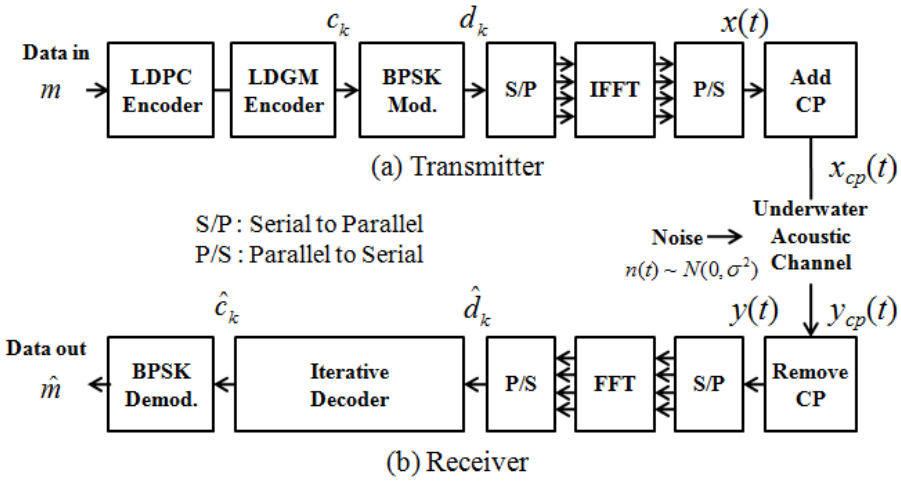

Figure 4.7 Block diagram of LDPC-LDGM coded OFDM system

Figure 4.7 is a block diagram of the suggested coded OFDM system using the regular LDPC-LDGM concatenated code. The major difference against block diagram of LDPC code OFDM system is that input data m is not a vector no more. In this section, the input data m is two dimension matrix size number of sub-carrier/LDPC code rate by number of sensor node. Others are exactly same with previous setting, only expect the input date is encoded by LDGM encoder, as well as is encoded by LDPC encoder.

In this section, since we aimed to overcome lognormal fading effect via spacial diversity based on LDGM code, we modeled simulation channel as lognormal fading channel mentioned above section 3.4 and verify robust performance.

4.2.4 LDGM code Parameter Setting

Table 4.1 LDGM code parameters

Parameter	Value
Type	*Regular*
Number of nodes : *m*	[10, 30, 50, 100]
Block size : *n*	2*m*
Degree : *D*	9
Relay choice method	Random selection

When designing the LDGM code, the performance of an LDGM ensemble is closely related to its degree. The larger the degree has the worse the waterfall performance but the lower the error floor [29]. Through the following Figure 4.8, we verified such trade-off relationship. We set the degree as 9 to lower the error floor but set as 5 in case of the number of nodes is equal to 10. In addition, since we assumed each node is able to receive and recovery all OFDM symbols from others nodes, we chose the relay randomly.

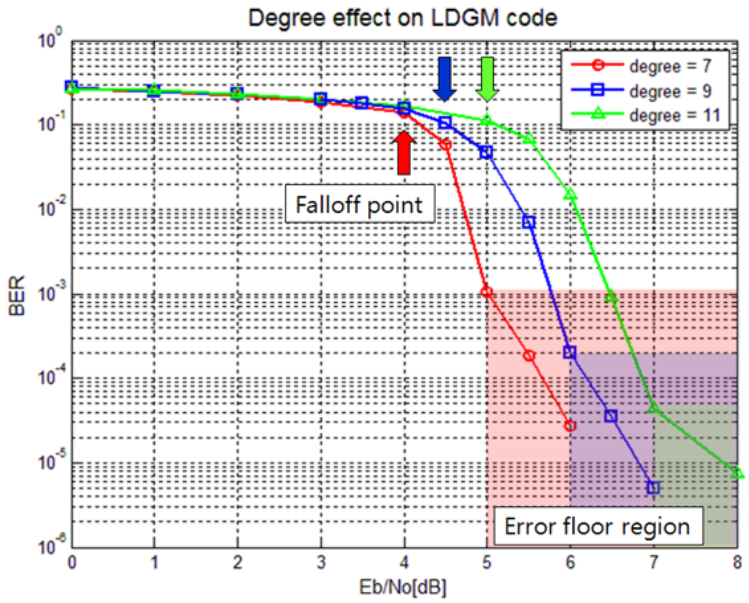

Figure 4.8 Degree effect in LDGM code

4.2.5 Performance Verification

Figure 4.9 and Figure 4.10 show the performance of designed LDPC-LDGM coded OFDM system over Non-lognormal fading UAC. Specially, Figure 4.9 is focused on the performance comparison versus un-coded OFDM system and Figure 4.10 has viewpoint on the performance change according to number of node.

As shown in Figure 4.9, under non-lognormal fading condition, suggested LDPC-LDGM coded OFDM system obtained 10^{-3} BER performance on about 6 dB SNR (there are a minor difference according to number of node), which is 17 dB lower SNR than un-coded OFDM system. Moreover, we verified performance improvement according to number or cooperation node through Figure 4.10. When we set 10^{-3} BER point as a criterion, 10 nodes cooperation LDPC-LDGM coded OFDM system is improved little but case of 100 nodes cooperation LDPC-LDGM coded OFDM system obtained additional 2 dB benefit versus LDPC coded OFDM system (i.e., LDPC-LDGM coded OFDM system can obtain same BER performance as the 2 dB lower SNR).

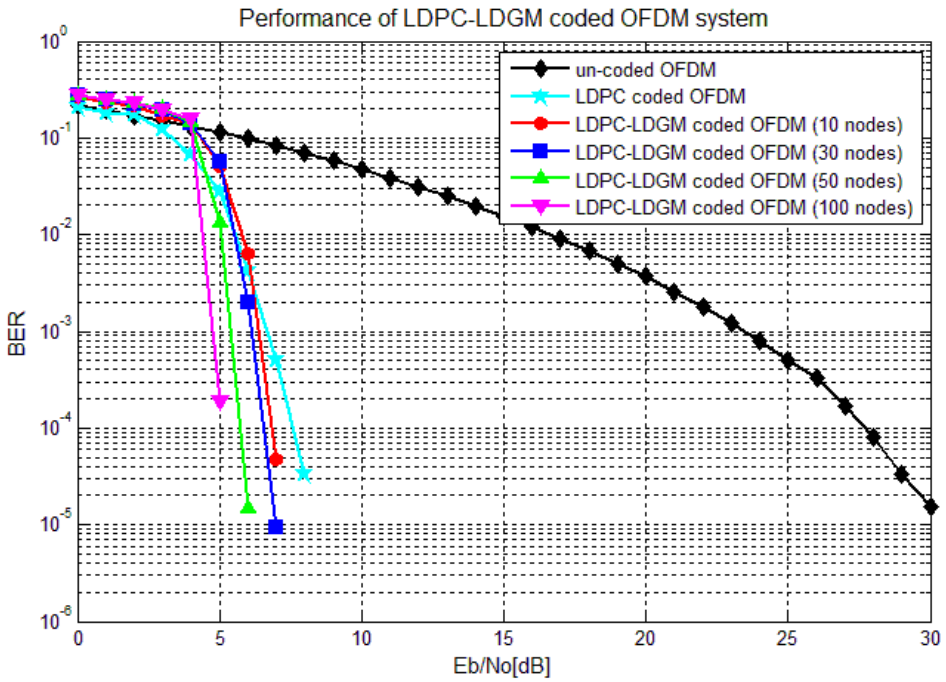

Figure 4.9 Performance of LDPC-LDGM coded ODFM system (Non-lognormal fading)

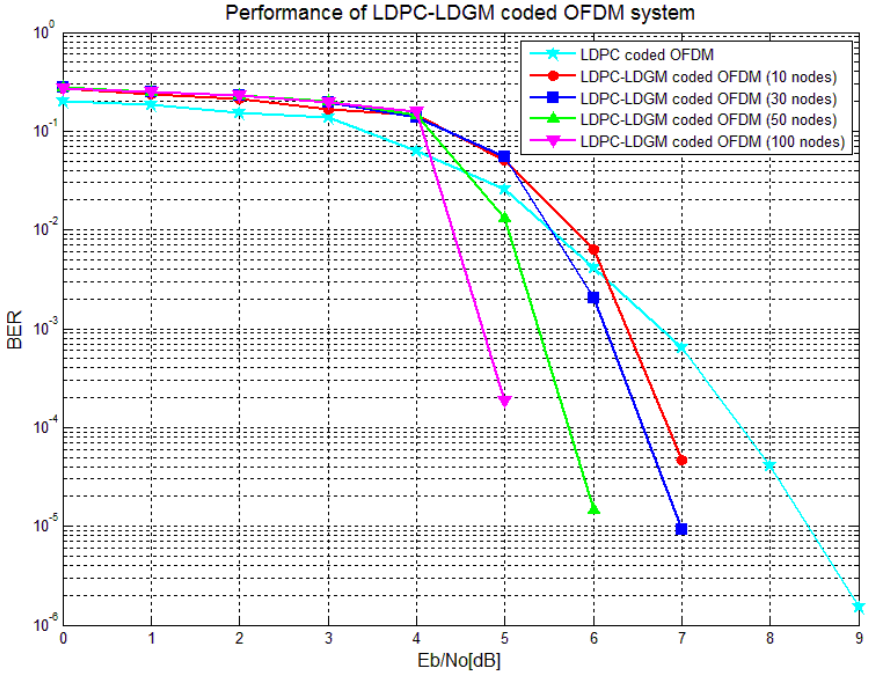

Figure 4.10 Performance of LDPC-LDGM coded ODFM system (Non-lognormal fading)(Zoom)

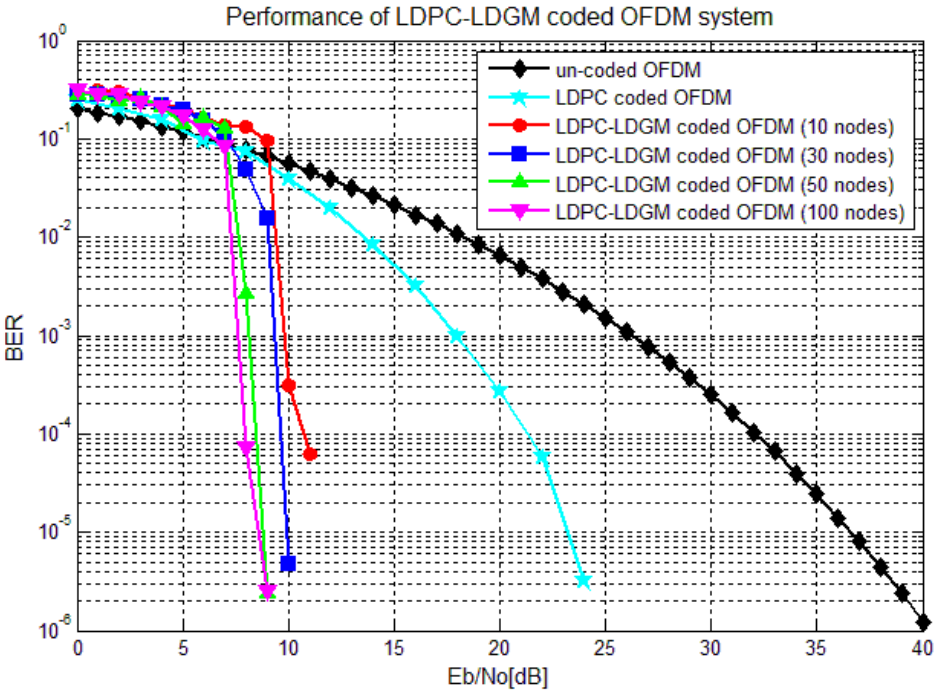

Figure 4.11 Performance of LDPC-LDGM coded ODFM system (Lognormal fading)

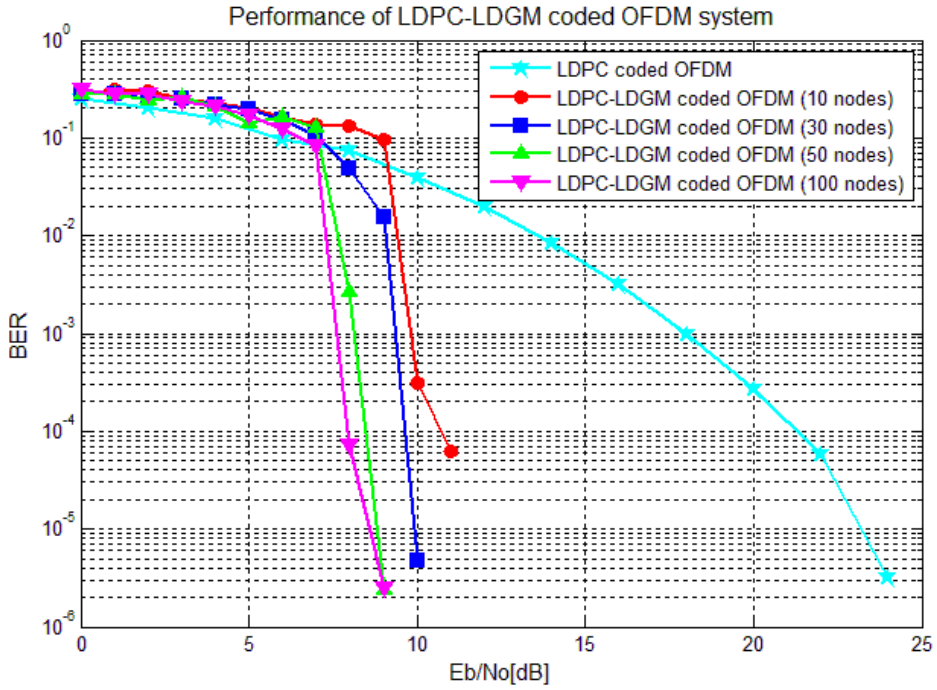

Figure 4.12 Performance of LDPC-LDGM coded ODFM system (Lognormal fading)(Zoom)

Similarly, Figure 4.11 and Figure 4.12 show the performance of designed LDPC-LDGM coded OFDM system over lognormal fading UAC. Specially, Figure 4.11 is focused on the performance comparison versus un-coded OFDM system in lognormal fading condition and Figure 4.12 has viewpoint on the performance change according to number of node.

As shown in Figure 4.11, under lognormal fading condition, designed LDPC-LDGM coded OFDM system obtained 10^{-3} BER performance on about 8 dB SNR (there are a minor difference according to number of node), which is 18 dB lower SNR than un-coded OFDM system. Moreover, we verified performance improvement according to number or cooperation node through Figure 4.12. Under the lognormal fading, i.e., resemble realistic channel, LDPC-LDGM coded OFDM system whatever using 10, 30, 50 and 100 nodes showed the performance improvement certainly versus LDPC coded OFDM system. As a detail, when we set 10^{-3} BER point as a criterion, 100 nodes cooperation LDPC-LDGM coded OFDM system obtained additional 10 dB benefit versus LDPC coded OFDM system.

5 Simulation Results and Discussion

Figure 5.1 and Figure 5.2 denotes the system performance according to coded scheme (i.e., un-coded, LDPC coded and LDPC-LDGM coded system), number of node (i.e., 10, 30, 50 and 100) and fading type (i.e., non-lognormal and lognormal fading). Although LDPC coded OFDM system shows the robust BER performance under non-lognormal fading condition, system performance falloff from 7 dB to 18 dB at the 10^{-3} BER point under lognormal fading condition. Contrastively, LDPC-LDGM coded OFDM system shows only small performance change from about 6 dB to about 8 dB due to effect of spacial diversity, which means LDPC-LDGM coded OFDM system based on multiple sensor networks offers not only outstanding but also robust performance in UAC. The designed system obtained about 18 dB benefits on power consumption versus un-coded OFDM system in whatever lognormal fading or not.

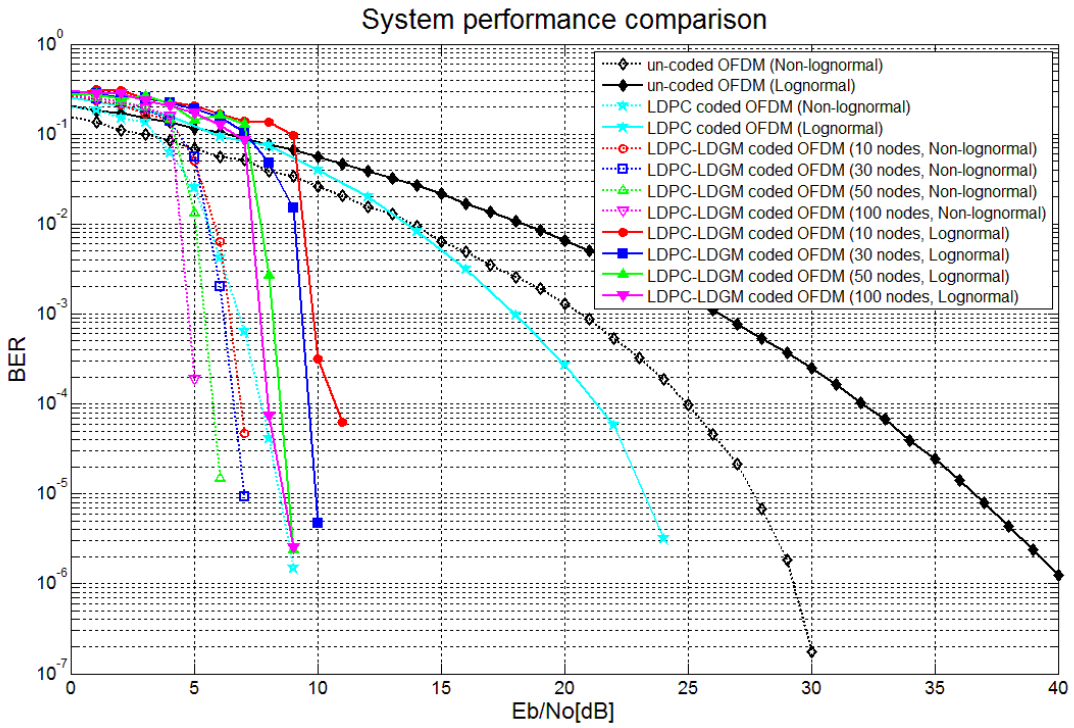

Figure 5.1 System performance comparison

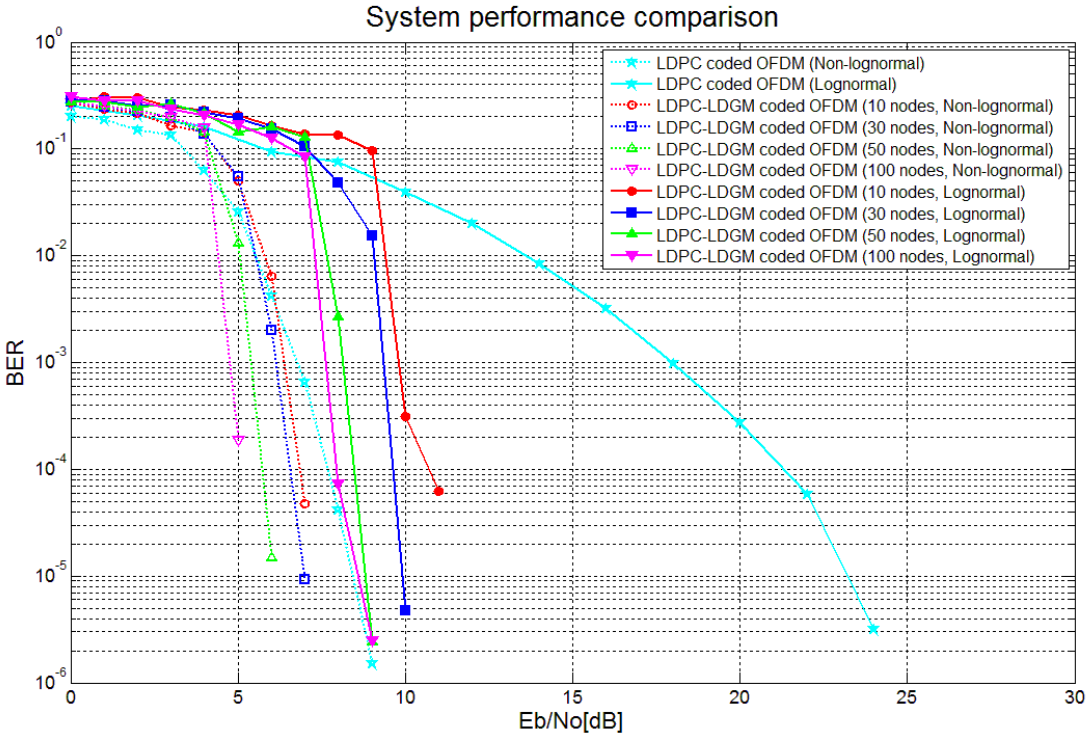

Figure 5.2 System performance comparison(Zoom)

6 Conclusion and Future Works

So far, we discussed communication system design in underwater. First of all, we dealt with channel analysis and channel modeling based on characteristics of UAC. The simulation channel modeled under assuming poor conditions like as 15 m/s maximum wind speed on sea surface, a number of reflected multipath, etc.

To set up a robust peer-to-peer communication system, we used OFDM technique and set the OFDM system parameter carefully to overcome ISI problem, frequency selective fading and time selective fading without additional frequency offset correction. In this process, we considered trade-off relationship between carrier frequency and Doppler spread. In addition, we combined LDPC codes with designed OFDM system to mitigate negative effect on certain sub-carriers fallen in deep fading.

As a next sequence, we expanded the system to multiple sensor networks. We designed LDPC-LDGM coded OFDM system that is encoded via LDPC codes on frequency domain and LDGM codes on spacial domain and verified system performance according to number of node (i.e., 10, 30, 50 and 100) and fading type (i.e., non-lognormal and lognormal fading). Finally, we identified that LDPC-LDGM coded OFDM system based on multiple sensor networks offers not only outstanding but also robust performance in UAC.

In this paper, we aimed to designed robust communication system only. Thus, there are many opened research clues, e.g., modulation method, macro and micro scatter in channel modeling, error floor problem in simulation, etc.

- Modulation method – Since the main goal of this paper is focused on not increasing transmission rate but designing robust performance, we used the basic modulation scheme, i.e., BPSK modulation. In such reason transmission rate is not good. For high speed communications, try to using other modulation methods like as quadrature phase shift keying (QPSK) and quadrature amplitude modulation (QAM) is requested.

- More detail channel modeling – In this paper, we assumed flat condition on sea surface and ocean bottom to simplify creation of reflection path. Under such assumption, there is no macro and micro scattering occurrence. There is a paper that used the more detail simulation channel considering such macro and micro scattering occurrence [16], which almost match up with measured data. For more realistic channel modeling, such factors should be considered.

- Error floor problem – When we simulated designed system based on LDGM codes in the MATLAB, some error floor was found. Such problem is one of the LDGM codes characteristics. Such error floor problem can be solved by using Raptor codes.

- Adaptive system parameter setting – In this paper, we set the simulation channel and set the parameters as analyzing simulation results of modeled channel, which is not adaptive. When we change the system parameter, e.g., distance between node and buoy, depth of water, etc., we should simulate and set the new parameters again. To reduce such repetition, trying to find general relationship between channel conditions and system parameters is necessary.

Reference

1. I. F. Akyildiz, D. Pompili, and T. Melodia, “Underwater acoustic sensor networks: research challenges,” *Ad Hoc Networks Journal*, Elsevier, vol. 3, Issue 3, pp. 257-279, Mar. 2005.
2. D.B. Kilfoyle and A.B. Baggeroer, “The state of the art in underwater acoustic telemetry”, Jan. 2000.
3. Timothy F. Duda and Allan D. Pierce, *History of EnvironmentalAcoustics, 1960s to 2000s*. 2008.
4. R Palacios Trujillo, *Interference Cancellation and Network Coding for Underwater Communication Systems*, 2010
5. Shengli Zhou Lanbo Liu and Jun-Hong Cui, *Prospects and Problems of Wireless Communication for Underwater Sensor Networks*, Wiley WCMC Special Issue on Underwater Sensor Networks (Invited), 2008.
6. I. F. Akyildiz, D. Pompili, and T. Melodia, “Challenges for efficient communication in underwater acoustic sensor networks,” *ACM SIGBED* Rev., vol. 1, no. 2, pp. 3-8, Jul. 2004.
7. M. Stojanovic and J. Preisig, “Underwater acoustic communication channels: Propagation models and statistical characterization,” *IEEE Communications Magazine*, vol. 47, no. 1, pp. 84-89, Jan. 2009.
8. Li-yang Bai, Fang Xu, Ru Xu, Shao-yu Zheng, "LDPC Application Based on CI/OFDM Underwater Acoustic Communication System," *icise*, 2009 First International Conference on Information Science and Engineering, pp.2641-2644, 2009.
9. J. Huang, S. Zhou, and P. Willett, “Nonbinary LDPC coding for multicarrier underwater acoustic communication,” *IEEE JSAC Special Issue on Underwater Wireless Communications and Networks*, vol. 26, no. 9, pp. 1684–1696, Dec. 2008.
10. P. Qarabaqi and M. Stojanovic, “Statistical modeling of a shallow water acoustic communication channel,” in *Proc. Underwater Acoustic Measurements Conference*, Nafplion, Greece, Jun. 2009.
11. L. Berkhovskikh and Y. Lysanov, *Fundamentals of Ocean Acoustics*, Springer, 1982.
12. Arshad Hussain, *Advanced RF Engineering for Wireless Systems and Networks*, Wiley, 2004.
13. R. Coates, *Underwater Acoustic Systems*, Wiley, 1989.

14. M. Stojanovic, “Underwater Acoustic Communication,” entry in *Encyclopedia of Electrical and Electronics Engineering*, John G. Webster, Ed., John Wiley & Sons, 1999, vol. 22, pp. 688-698.
15. M. Stojanovic, “On the Relationship Between Capacity and Distance in an Underwater Acoustic Communication channel,” in *Proc. First ACM International Workshkp on Underwater Networks (WUWNet)*, Sep. 2006.
16. Alenka G. Zajic, “Statistical Modeling of MIMO Mobile-to-Mobile Underwater Channels,” IEEE Trans. on Vehicular Technology, vol. 60, no. 4, May 2011.
17. M. Stojanovic, “Underwater Acoustic Communi-cations: Design Considerations on the Physical Layer,”*IEEE/IFIP First Annual Conference on Wireless on demand Network Systems and Services* (WONS 2008), Garmisch-Partenkirchen, Germany, Jan. 2008.
18. L. Litwin and M. Pugel, “The Principles of OFDM,” RF Signal Processing, pp. 30-48, Jan. 2001.
19. O. Edfors, M. Sandell, J. van de Beek, D. Landstrom, and F. Sjoberg, *An introduction to orthogonal frequency-division multiplexing*, Technical report, Lulea University of Technology, Sep. 1996
20. B. Sklar, *Digital Communications: Fundamentals and Applications*, 2nd Ed., Prentice Hall, 2001.
21. S. Mason, C. Berger, S. Zhou, K. Ball, L. Freitag, and P. Willett, “An OFDM design for underwater acoustic channels with Doppler spread,” in Proc. of the 13th DSP Workshop, Marco Island, FL, Jan. 2009.
22. M. Stojanovic, “OFDM for underwater acoustic communications: Adaptive synchronization and sparse channel estimation,” in Proc. of International Conference on Acoustics, Speech and Signal Proc., Apr. 2008.
23. M. Stojanovic, “Low complexity OFDM detector for underwater channels,” in Proc. of MTS/IEEE OCEANS conference, Boston, MA, Sep. 2006.
24. I. F. Akyildiz, D. Pompili, and T. Melodia, “Challenges for efficient communication in underwater acoustic sensor networks,” *ACM SIGBED* Rev., vol. 1, no. 2, pp. 3-8, Jul. 2004.
25. R. G. Gallager, “Low density parity check codes,” IRE Trans. Inform. Theory, vol. IT-8, pp. 21-28, Jan. 1962.
26. S. ten Brink, G. Kramer, and A. Ashikhmin, “Design of Low-Density Parity-Check Codes for Modulation and Detection,” IEEE Trans. Commun., vol. 52, pp. 670-678, Apr. 2004.

27. H. N. Lee, *Wireless Communications* Class lecture notes, GIST, spring semester, 2010.

28. Evans, M., N. Hastings, and B. Peacock. *Statistical Distributions*. Hoboken, NJ: Wiley-Interscience, 2000.

29. X. Bao, and J. Li, "Matching Code-on-Graph with Network-on-Graph: Adaptive Network Coding for Wireless Relay Networks," Proc. Allerton Conf. on Commun. Control and Computing IL, Sept. 2005.